



Batchelor Prize Lecture: Measurements in wall-bounded turbulence

Alexander J. Smits[†]

Department of Mechanical and Aerospace Engineering, Princeton University, Princeton, NJ 08544, USA

(Received 6 January 2022; revised 18 January 2022; accepted 19 January 2022)

Our understanding of turbulent boundary layer scaling and structure has advanced greatly in the past 20 to 30 years. On the computational side, direct numerical simulations and large-eddy simulations have made extraordinary contributions as numerical methods and computational resources have advanced, while on the experimental side major advances in instrumentation have made available new imaging and quantitative techniques that provide unprecedented accuracy and detail. Here, I illustrate how the development of such experimental methods have aided our progress by reference to some particular topics related to the structure of turbulent boundary layers: the power law scaling of the mean velocity and its relationship to the mesolayer; the scaling of the outer layer with regard to the log law in turbulence; the development of the outer peak; and the scaling of the turbulent stresses in the near-wall region, with an emphasis on the streamwise component.

Key words: boundary layer structure, pipe flow boundary layer, turbulent boundary layers

1. Introduction

Over the past 20 or 30 years, our understanding of the scaling and structure of wall-bounded turbulent flows has advanced greatly. Direct numerical simulations (DNS) and large-eddy simulation have made extraordinary contributions to our understanding as computational resources have exploded and numerical methods continue to evolve, while experiments have benefited from advances in instrumentation that have provided unprecedented accuracy and detail. We have also seen an intimate convergence of experiment and computation that has accelerated progress even further. In particular, canonical wall-bounded flows such as flat plate, zero pressure gradient boundary layers and fully developed pipe and channel flows are now known to display many similarities in the scaling of their mean velocity and turbulence distributions, and this convergence is

[†] Email address for correspondence: asmits@princeton.edu

A video of the Batchelor Prize Lecture, delivered at the ICTAM 2020+1 virtual meeting, can be found at www.cambridge.org/bachelor_prize_2020.

especially clear at high Reynolds number. Here, we focus on some of the contributions made by experiment to this progress in understanding.

Measurements in turbulence rely on three basic tools: hot-wire anemometry; laser Doppler velocimetry (LDV); and particle image velocimetry (PIV). Pitot probes are also often used to measure the local dynamic pressure, and when combined with a separate measurement of the static pressure (often achieved using a static pressure tap in the wall) will yield the local mean velocity. Hot-wire anemometry uses a heated wire sensor that is inserted into the flow field, and by monitoring the voltage supplied to the sensor to keep either its resistance or its current constant the instrument provides (using a suitable calibration technique) a continuous time history of the flow velocity at a point. It is possible to measure different components of the velocity fluctuations by using multiple sensors, but in its most common form (the normal wire) it measures only the streamwise component. This method has a long history, and there is a wealth of literature available on its strengths and limitations (see, for example, Comte-Bellot 1976; Freymuth 1978; Perry 1982; Smoliakov & Tkachenko 1983; Lomas 1986; Fingerson 1994; Bruun 1995).

In LDV and PIV, the flow is seeded with small particles and their motion is tracked using optical methods. Both LDV and PIV are considered to be non-intrusive methods, in that there is no physical sensor present in the flow. In LDV, the measurement volume is defined by the crossing of a pair of focused laser beams, and a single velocity component is found by recording the Doppler shift in the scattered light as particles pass through the measurement volume (see, for instance, Adrian & Goldstein 1971; George & Lumley 1973; Durst, Melling & Whitelaw 1976; Tropea 1995). It is possible to measure more than one component of velocity by collocating the measurement volumes created by multiple pairs of laser beams. In PIV the seeding particles are illuminated by a light emitting diode or laser sheet, and by using a camera to record two successive images of the particles the velocity at any point in the imaged field can be found by correlation or particle tracking techniques. The method yields two components of the velocity fluctuations at the same time, and by using two cameras it can also give the third component in the plane of the laser sheet (this is called stereo PIV or sPIV). Tomographic and holographic techniques can extend the data to a volume, although PIV is used most commonly in its planar or stereo mode. Its application has blossomed since its introduction in the early 1980s, and it has had a major influence on our ability to measure and visualize turbulence (Adrian 1984; Adrian & Westerweel 2011; Westerweel, Elsinga & Adrian 2013).

A comprehensive review of these techniques is well beyond the scope of the present contribution. Instead, I consider how recent advances have helped to answer some key questions on how turbulent wall-bounded flow develops with Reynolds number. This quest naturally prioritizes studies at high Reynolds number so that scaling trends can be identified, and there is always an underlying need for accuracy since we know from experience that such variations are subtle. My survey is rather selective, in that I am primarily concerned with statistical measures of turbulence, and the particular topics are framed in terms of the expectations derived from theory or scaling arguments. We start with mean flow considerations before tackling the turbulent stress behaviour.

2. Mean flow scaling

One of the landmark results in wall-bounded turbulence is the presence of a logarithmic region in the mean velocity (Prandtl 1925; von Kármán 1930). It is often cast as a region of overlap (Millikan 1938), where the inner-scaled wall region overlaps with the outer-scaled

outer region. In general we write, for isothermal, incompressible, wall-bounded flow

$$[U_i, \overline{u_i u_j}] = f(y, u_\tau, \nu, \delta), \tag{2.1}$$

where U_i and u_i are the mean and fluctuating velocities in the i th direction, and y is the distance from the wall. The overbar denotes time averaging, and δ is, as appropriate, the boundary layer thickness, the pipe radius, or the channel half-height. The friction velocity $u_\tau = \sqrt{\tau_w/\rho}$, where τ_w is the wall stress and ρ and ν are the fluid density and kinematic viscosity, respectively. Equation (2.1) assumes that there is only a single velocity scale for the entire layer, given by u_τ . A separate outer velocity scale, u_0 , was proposed by Zagarola & Smits (1998a), where $u_0 = U_\infty \delta^*/\delta$ (U_∞ is the free stream or centreline velocity and δ^* is the displacement thickness). For pipe flows and boundary layers, the collapse of the mean velocity was noticeably improved when using u_0 instead of u_τ for $y/\delta > 0.07$ and for $650 < Re_\tau < 18 \times 10^3$ (Zagarola & Smits 1998a,b). At higher Reynolds numbers, however, u_0 becomes proportional to u_τ so that it appears that u_τ can be used to scale both the inner and outer layers if the Reynolds number is sufficiently high. By dimensional analysis, we can then write the functional dependence given by (2.1) in two ways,

$$[U_i^+, \overline{u_i u_j}^+] = f(y^+, Re_\tau) \tag{2.2}$$

or $[U_i^+, \overline{u_i u_j}^+] = f(y/\delta, Re_\tau), \tag{2.3}$

where the friction Reynolds number is $Re_\tau = \delta u_\tau/\nu$ and the superscript ‘+’ denotes non-dimensionalization by the velocity scale u_τ and the ‘inner’ length scale ν/u_τ (for example, $y^+ = yu_\tau/\nu$). Near the wall the inner length scale is of the same order as the Kolmogorov length scale η , and so it is characteristic of the smallest scales in the flow, while the outer length scale δ is a measure of the largest scales. The friction Reynolds number therefore measures the separation between the largest and smallest scales. The form given by (2.2) is called inner scaling, and that given by (2.3) is called outer scaling. For convenience, we will use U for the mean and u for the fluctuating velocity component in the streamwise direction, and so the corresponding non-dimensional stress is given by $\overline{u^2}^+ = \overline{u^2}/u_\tau^2$.

The central role of the Reynolds number is clear from (2.2) and (2.3): as the Reynolds number goes to very large values, these relationships imply that the inner part of the flow becomes a function of y^+ only and the outer flow becomes a function of y/δ only. At sufficiently high Reynolds number, Millikan (1938) proposed that there may be a region that spans $y^+ \gg 1$ and $y/\delta \ll 1$ where (2.2) and (2.3) overlap. By assuming that Reynolds number effects are negligible and by matching the mean velocity gradients for the inner and outer regions in this ‘overlap’ region, we obtain

$$\frac{\partial U}{\partial y} = \frac{u_\tau}{\kappa y} = \frac{\sqrt{\tau_w/\rho}}{\kappa y}, \tag{2.4}$$

where κ is the von Kármán constant. For this overlap region, the length scale is simply the distance from the wall. By integration, we obtain the inner and outer forms of the log law for the mean velocity:

$$U^+ = \frac{1}{\kappa} \ln y^+ + B, \tag{2.5}$$

$$U_\infty^+ - U^+ = -\frac{1}{\kappa} \ln y/\delta + B_1. \tag{2.6}$$

Note that the additive constant B depends on the lower limit of integration in y and so it may depend on Reynolds number (see, for example, Duncan, Thom & Young

1970; Schlichting 1979; Zagarola & Smits 1998a). For all reasonable Reynolds numbers, however, it appears that B can be assumed to be constant.

The log law for the mean velocity was derived as early as 1925 by Prandtl using his mixing length theory combined with the assumption of constant stress (Prandtl 1925). A few years later, Nikuradse's measurements in a pipe provided extensive data to support the presence of this log law, with constants $\kappa = 0.4$ and $B = 5.5$ (Nikuradse 1932). Can new experiments add anything to this almost totemic result? As it turns out, they can contribute much.

3. Mean flow measurements

There are three basic requirements for any serious investigation of the log law for the mean velocity. First, the friction velocity must be known accurately because it is a crucial scaling parameter. Second, the Reynolds number must be sufficiently high so that there is adequate separation between the inner and outer scales. Third, precise measurements of the velocity are necessary to deduce the slope of the line, that is, von Kármán's constant κ , since the errors that arise from differentiating discrete data are well known. In addition, any error in evaluating κ will also affect the deduced value of the additive constant B .

To satisfy the first criterion, the preferred flow configuration is either fully developed pipe or channel flow because the friction velocity can be found with high precision by simply measuring the pressure drop (for pipes $u_\tau^2 = -(D/4) dp/dx$, where dp/dx is the pressure gradient). Direct and accurate measurements of the friction velocity in boundary layers is much more difficult, although oil drop methods have made considerable progress (Naughton & Sheplak 2002; Segalini, Rüedi & Monkewitz 2015; Lee *et al.* 2019).

To satisfy the criterion for high Reynolds number, a number of new, purpose-built facilities are now available, as discussed by Smits (2020). The older facilities capable of reaching high Reynolds numbers were largely designed for aeronautical or atmospheric flow investigations, and usually did not have the required flow quality for fundamental turbulent boundary layer studies. The newer facilities include the Princeton SuperPipe (Zagarola & Smits (1998a); figure 1a), the Stanford high-pressure tunnel (De Graaff & Eaton 2000), the Princeton High Reynolds number Testing Facility (HRTF) (Jiménez, Hultmark & Smits 2010), the high Reynolds number boundary layer wind tunnels at the University of New Hampshire (Vincenti *et al.* 2013) and the University of Melbourne (Marusic *et al.* (2015); figure 1b), the large-scale pipe flow facility at the Center for International Cooperation in Long Pipe Experiments (CICLoPE) (Örlü *et al.* 2017; Willert *et al.* 2017) and the pipe flow experiments at the National Metrology Institute of Japan (NMIJ) (Furuichi, Terao & Tsuji 2017; Furuichi *et al.* 2018). The first three use high-pressure air as the working fluid to achieve high Reynolds number, whereas the others use air at atmospheric pressure, except for the NMIJ pipes which use water. The SuperPipe, CICLoPE and NMIJ were built to study pipe flows, while the others were focused on boundary layers. There are no channel flow facilities with sufficiently high Reynolds number to provide definitive evidence for Reynolds number trends. There are good reasons for this, as discussed in part by Vinuesa *et al.* (2014), but it is nevertheless somewhat unfortunate given that DNS has mostly focused on two-dimensional channel flows.

To help satisfy the third criterion for precise measurements of velocity, Bailey *et al.* (2013) examined ways for making Pitot tubes more accurate, while also evaluating the performance of hot-wire probes for mean velocity measurements. They found that with careful attention to all the sources of error the two techniques could give mean velocity data to within 1% of each other over most of the velocity profile. The Pitot probe is

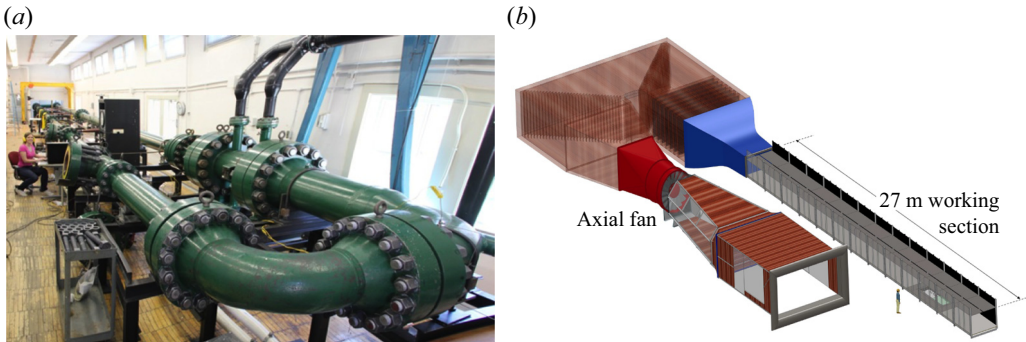


Figure 1. High Reynolds number test facilities. (a) Princeton SuperPipe covering the range $1000 \leq Re_\tau = 500\,000$ (Zagarola & Smits 1998a). (b) Melbourne University High Reynolds Number Boundary Layer Wind Tunnel covering the range $2000 \leq Re_\tau \leq 30\,000$ (Marusic *et al.* 2015).

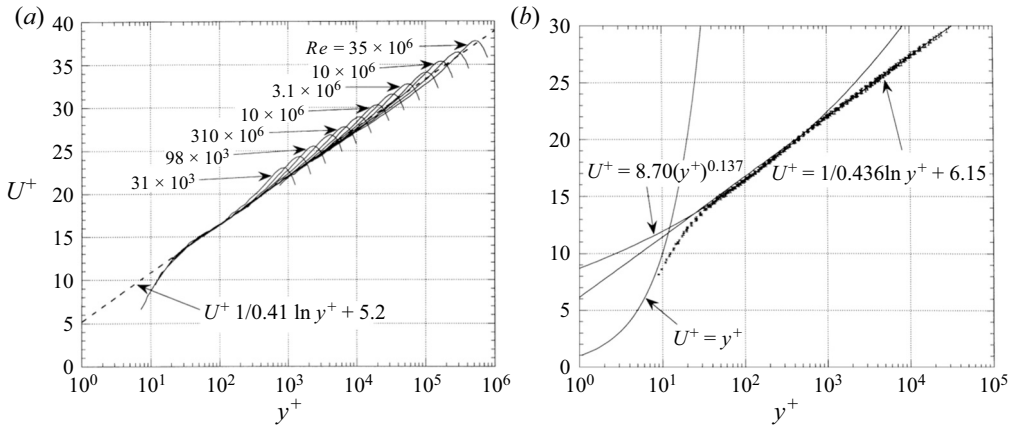


Figure 2. Semilogarithmic plots of the velocity profile data from the Princeton SuperPipe for Reynolds numbers from $Re_\tau = 1700$ to $503\,000$: (a) complete profiles; (b) profiles within $0.07Re_\tau$ of the wall. Adapted from Zagarola & Smits (1998a) and McKeon *et al.* (2004).

often preferred over the hot wire because of its inherent simplicity and straightforward implementation. However, it is necessary to make a number of corrections to the raw data to allow for: (i) effects that appear when the Reynolds number based on tube diameter is below 100 (MacMillan 1954; Zagarola & Smits 1998a); (ii) shear or velocity gradient effects that account for streamline deflection due to the presence of the probe (MacMillan 1957; McKeon *et al.* 2003); (iii) near-wall effects (MacMillan 1957; McKeon *et al.* 2003); and (iv) turbulence effects which tend to augment the inferred dynamic pressure (Bailey *et al.* 2013). Such corrections are relatively straightforward, except possibly the turbulence correction where some prior estimate of the turbulence needs to be on hand. For canonical wall-bounded flows this is not a problem. Finally, the static pressure measured by a static tap is subject to viscous effects and will also require a Reynolds-number-dependent correction (Franklin & Wallace 1970; McKeon & Smits 2002).

The Pitot tube velocity profiles taken in the Princeton SuperPipe are shown in figure 2 for $Re_\tau = 10^3$ to 5×10^5 . At first sight, we see an extended logarithmic region, although it is not fitted well by using $\kappa = 0.41$ and $B = 5.2$ (the values suggested by De Brederode & Bradshaw (1974) as the best fit to the extant published data). A closer observation shows

that for the region encompassing approximately $50 < y^+ < 300$ the velocity variation is better represented by a power law than a log law (figure 2*b*).

In this respect, Zagarola & Smits (1998*a,b*) noted that the overlap argument that led to the log law description can be constrained further by requiring the velocity magnitude to match in addition to the velocity gradient. Then the result is not a log law but a power law given by

$$U^+ = C_1(y^+)^{\gamma}, \quad (3.1)$$

(see also George & Castillo 1997). For pipe flow, Zagarola & Smits (1998*a*) found that this power law applied over the region $50 < y^+ < 300$ with $C_1 = 8.70$ and $\gamma = 0.137$ (independent of Reynolds number), as shown in figure 2(*b*). The later investigation by McKeon *et al.* (2004) yielded $C_1 = 8.47$ and $\gamma = 0.142$. Both studies found that the log law was present at higher Reynolds numbers, but only for $y^+ \gtrsim 600$. These observations were in direct contrast to the conventional wisdom at the time, which held that the log law for all wall-bounded flows started at approximately $y^+ = 30$ (Pope 2000), or possibly 70 (Schlichting 1979). The SuperPipe data demonstrated that the log law in the mean velocity only emerges at very high Reynolds numbers. For example, given that the log law for pipe flow begins at approximately $y^+ = 600$ and ends at $y/\delta = 0.12$ (McKeon *et al.* 2004), a log law would occur over a decade in y^+ only when $Re_{\tau} > 50\,000$. For an octave of log law, we would need $Re_{\tau} > 10\,000$.

The corresponding uncertainty in evaluating von Kármán's constant from experimental data was examined by Bailey *et al.* (2014). By comparing multiple measurements of the mean velocity profile in the Princeton SuperPipe using both Pitot tubes and hot wires it was concluded that $\kappa = 0.40 \pm 0.02$, a much higher level of uncertainty than initially reported by McKeon *et al.* (2004). This uncertainty exists even though in pipe flow u_{τ} can be determined to within 1% (Zagarola & Smits 1998*a*). Similar observations most likely apply to the experimental value of κ reported for boundary layers and channels, despite some reports to the contrary (Zanoun, Durst & Nagib 2003; Nagib & Chauhan 2008). Bailey *et al.* (2013) also found that κ was not very sensitive to using different end points for the log law (in the range $y/R = 0.1\text{--}0.15$), and that the start of the log law did not appear to be Reynolds number dependent.

What about computation? In DNS, as elsewhere, the region of logarithmic variation and the value of κ are often found by examining the so-called indicator function, $y^+(\partial U^+/\partial y^+)$, which is equal to $1/\kappa$ in the region where a log law is present. Channel flow DNS consistently gives κ values between 0.38 and 0.39 (see, for example, Lee & Moser 2015; Yamamoto & Tsuji 2018; Hoyas *et al.* 2022), but it is also clear that the region where the velocity profiles follow the log law is of very limited extent, and the behaviour at higher Reynolds number is not obvious. This is illustrated in figure 3 for the channel flow DNS by Lee & Moser (2015). The indicator function behaviour demonstrates that even at $Re^+ = 5200$, the logarithmic region, if it exists at all, occupies a very small extent in y^+ . In fact, we see from figure 3(*b*) that the power law given by (3.1) fits the channel flow data well for all Reynolds numbers up to $Re_{\tau} = 5200$, suggesting that the logarithmic law has not yet appeared.

4. Turbulent stress scaling

Like the mean velocity, the scaling of the turbulent stresses is also considered separately for the inner and outer regions, as given by (2.2) and (2.3). We first address the behaviour in the overlap region and then focus more particularly on the scaling of the inner region where the streamwise stress displays a strong maximum.

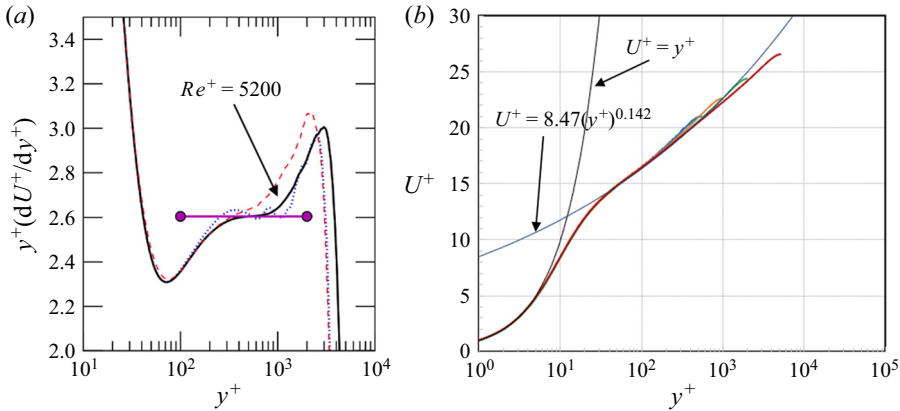


Figure 3. Mean velocity results from DNS of channel flow at $550 \leq Re_\tau \leq 5200$ (Lee & Moser 2015). (a) Log law indicator function at $Re_\tau = 5200$. The horizontal line corresponds to $\kappa = 0.384$. Figure adapted from Lee & Moser (2015) with permission. (b) Semilogarithmic plots showing fit to (3.1) for $Re_\tau = 550, 1000, 2000, 5200$.

In the overlap region, if we make the same argument as that given for the mean flow, we obtain for the streamwise component of the turbulent stress

$$\frac{\partial \overline{u^2}}{\partial y} = -\frac{u_\tau^2}{A_1 y}, \quad (4.1)$$

where A_1 is the Townsend–Perry constant (the negative sign is introduced for later convenience). This result is obtained by matching the gradients of $\overline{u^2}$ as obtained from the inner and outer representations and assuming that Reynolds number effects are negligible. Equation (4.1) can be integrated to give a log law for the turbulence intensity distribution in either inner- or outer-layer coordinates. However, some major caveats need to be taken into account. The same overlap argument would yield a logarithmic dependence for all higher-order moments, and for all three components of the Reynolds stress as well as the turbulent shear stress $-\overline{uv}$. Such inferences always need to be tested by experiment, but we already know that the result for the shear stress is incorrect; an order-of-magnitude analysis applied to the Reynolds-averaged momentum equation for boundary layers in a zero pressure gradient indicates that there exists a region of constant stress ($\tau_w = -\rho \overline{uv}$) near the wall, which includes the region of overlap. If the pressure gradient is not zero, as is the case for channel and pipe flow, then the extent of this constant stress region may be reduced, or the total stress may vary somewhat across this region. Either effect is usually ignored, and the overlap region is therefore often assumed to be a region where $-\overline{uv}$ is constant and equal to u_τ^2 (see also Johnstone, Coleman & Spalart 2010). That is, the shear stress does not follow a log law in the overlap region, despite the leeway for an overlap argument.

It is also possible to use different matching conditions in the overlap region. As in the case of the velocity profile, if we match both gradients and magnitudes we obtain a power law for the turbulence, and if we match only the magnitudes we would find a region where the stresses are constant. There is no experimental support for the power law behaviour in the stresses, but we have already noted that the shear stress is constant in this region, at least at higher Reynolds numbers, and $\overline{v^2}$ follows a similar behaviour. Tantalizingly, $\overline{u^2}$ at high Reynolds number seems to flirt with a region of constancy in the neighbourhood

of $y^+ \approx 100$, although this may simply be a result of a transition from viscous to inviscid dependence.

In this respect, Townsend's attached eddy hypothesis gives much-needed physical insight. He wrote: 'It is difficult to imagine how the presence of the wall could impose a dissipation length scale proportional to distance from it unless the main eddies of the flow have diameters proportional to distance of their "centres" from the wall, because their motion is directly influenced by its presence. In other words, the velocity fields of the main eddies, regarded as persistent, organized flow patterns, extend to the wall and, in a sense, they are attached to the wall' (Townsend 1976). He then supposed that the main energy-containing motions are made up of contributions from such attached eddies with similar velocity distributions, with their arrangement chosen so that $-\overline{uv} = u_\tau^2$. This inviscid model, valid in the constant stress region of the boundary layer, yields

$$\overline{u^2}^+ = B_1 - A_1 \ln(y/\delta) - V(y^+), \quad (4.2)$$

$$\overline{w^2}^+ = B_2 - A_2 \ln(y/\delta) - V(y^+), \quad (4.3)$$

$$\overline{v^2}^+ = A_3 - V(y^+), \quad (4.4)$$

where the function $V(y^+)$ was introduced by Perry, Henbest & Chong (1986) and Perry & Li (1990) to account for viscous effects at lower Reynolds numbers. According to this model, the streamwise and spanwise stresses follow a log law at sufficiently high Reynolds number, but the wall-normal fluctuations do not. They also noted that the model is envisaged to apply for $y^+ \geq 100$; $y/\delta < 0.15$, and that B_i and A_i are expected to be universal constants for a given flow. As Perry & Li (1990) point out, one of the consequences of (4.2)–(4.4) is that there is no 'law of the wall' for $\overline{u^2}^+$ or $\overline{w^2}^+$ but there should be one for $\overline{v^2}^+$. That is, there is no 'inner' equivalent of (4.2) and (4.3), even though (4.1) is open to that possibility.

For the logarithmic terms to emerge clearly we need $V(y^+)$ to become negligible, which will only happen at high Reynolds number. In addition, the log law for turbulence (4.2) may reasonably be expected to coexist with the log law in the mean velocity (as argued by Perry *et al.* (1986)), which also requires high Reynolds numbers. In this respect, Marusic, Uddin & Perry (1997) did not find any significant region of log law in measurements of $\overline{u^2}^+$ conducted at $Re^+ = 4704$, at least to the extent necessary to determine the constants to a reasonable accuracy. A similar conclusion was made by Lee & Moser (2015) in DNS of channel flow at $Re^+ = 5200$, although they found support for a log law distribution of the spanwise component (4.3). Such investigations have since been aided by the development of special-purpose, high-quality, high Reynolds number laboratory facilities, and by major improvements in turbulence instrumentation. We now consider these instrumentation developments, with a particular focus on hot-wire anemometry.

5. Turbulent stress measurements

As noted earlier, measurements of the velocity fluctuations are most commonly made using hot-wire anemometry, LDV or PIV. All three methods are subject to limitations on spatial and temporal resolution which filter the signal and cause the measurements to underestimate their true value, especially near the wall where the spatial scales are small and the time scales are short. Therefore, the principal challenges with measuring turbulent stresses are to obtain adequate frequency response and to achieve sufficient spatial resolution.

5.1. Frequency response

The concept of hot-wire anemometry dates back at least to the late 1800s (Comte-Bellot 1976), but it was the work by King (1914) on the heat transfer from cylinders in cross-flow that put it on a firm theoretical and practical basis. In thermal anemometry the wire is heated by an electric current and cooled by the passing flow, and King's law relates the Nusselt number to the Reynolds number. The variations in the wire temperature cause its resistance to vary, and the voltage output is therefore a function of the velocity. One of the great advantages of hot-wire anemometry is that the output signal gives a continuous record of the velocity fluctuations so that the spectral content of the turbulence can be examined (up to the frequency response of the system).

The early devices were of all of the open-loop, constant-current type, and the frequency response was limited by the thermal inertia of the wire. That is, the system response was defined by the natural frequency of the wire, which is given by

$$f_R = \frac{4k_f}{\rho_w C_w} \frac{Nu}{d^2}, \quad (5.1)$$

where ρ_w and C_w are the wire material density and specific heat, respectively, Nu is the Nusselt number and k_f is heat conductivity of the fluid. A typical wire is made of platinum, with a length $\ell = 1$ mm and a diameter $d = 5$ μm , and so f_R is less than 100 Hz. The wire response approximates a simple pole so that f_R is the -3 dB point, where the amplitude of the signal has dropped by approximately 50%. To have less than 5% signal loss, therefore, the frequency content of the signal needs to be less than approximately $f_R/3$. This limit may be adequate for some applications, as in an atmospheric boundary layer experiment where the highest frequencies of interest may be < 30 Hz, but it is highly restrictive for most laboratory flows. There are obvious benefits to making the wire smaller, but for conventional wires the smallest diameter is set by limits based on strength.

A compensating network was therefore introduced by Dryden & Kueth (1929) where the network generates a zero in the frequency response which is then tuned to match the pole response of the wire. Subsequent refinements of this concept have extended the frequency response by more than two orders of magnitude, and such constant current systems are still used in some supersonic flow applications and for the measurement of temperature fluctuations (see, for example, Smits, Perry & Hoffmann 1978; Bestion, Gaviglio & Bonnet 1983; Barre *et al.* 1993; Williams, Van Buren & Smits 2015). In current practice, digital compensation has become a natural alternative to analogue networks (Briassulis *et al.* 1995).

The most common type of anemometer in contemporary use is the constant temperature system, where a high-gain feedback circuit is used to keep the wire resistance (that is, its temperature) constant even as the velocity fluctuates. In this way, the frequency response of the system can be increased by several orders of magnitude without manual intervention. The actual frequency response is difficult to measure directly and therefore it is often estimated using a square-wave response test (Perry 1982). This can be misleading. For example, Hutchins *et al.* (2015) used the Princeton SuperPipe to explore a number of flows at matched Reynolds numbers but with turbulent energy in different frequency ranges. The differences between the energy spectra for these flows then indicated the measurement errors as a function of frequency. They found that the frequency response of under- or over-damped systems in their tests was only approximately flat up to 5–7 kHz, despite more optimistic square-wave tests, and they suggested ways to improve the system response. This is discussed further below.

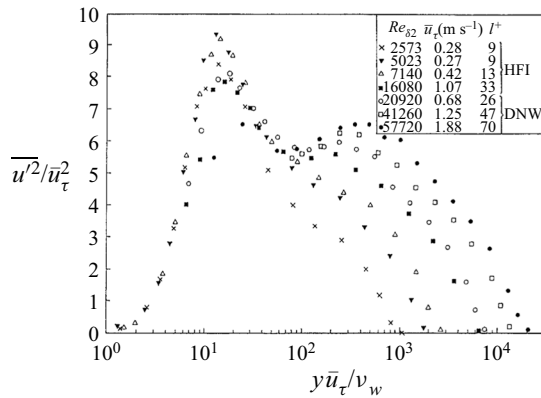


Figure 4. Streamwise turbulence intensity $\overline{u'^2}$ in boundary layers for $Re_\theta = 2573\text{--}57\ 720$; $Re_\tau = 1105\text{--}16\ 800$: (a) inner scaling – for the three highest Reynolds numbers, the outer peak is located at approximately $7\ell^+$; (b) outer scaling, where Δ is the Clauser thickness. Data from Bruns, Dengel & Fernholz (1992) (HFI) and Fernholz *et al.* (1995) (DNW). Adapted from Fernholz & Finley (1996) with permission.

5.2. Spatial resolution

In hot-wire anemometry the spatial resolution is usually expressed in terms of the non-dimensional wire length $\ell^+ = \ell u_\tau / \nu$. However, simply reducing ℓ^+ by making the wire length smaller while keeping its diameter constant is limited by the need to avoid end conduction effects that come into play when $\ell/d < 200$ (Ligrani & Bradshaw 1987; Hultmark, Ashok & Smits 2011). Because the minimum diameter is often set by strength requirements, there are natural limits on both ℓ and d .

Figure 4 illustrates well the effects of spatial filtering. These pioneering data, taken in the German–Dutch wind tunnel (DNW), were some of the first to document the turbulence behaviour in boundary layers at high Reynolds numbers, in this case up to $Re_\tau \approx 17\ 800$ (Fernholz & Finley 1996). The data display some characteristic features, starting with a pronounced peak in the turbulence intensity near $y^+ \approx 15$, the so-called ‘inner’ peak. Its magnitude, $\overline{u_p'^2}$, is seen to first rise and then fall with increasing Reynolds number. A second or ‘outer’ peak appears for $y^+ > 100$ and $Re_\tau > 5000$ ($Re_\theta > 16\ 000$). The appearance of the outer peak and the fall in $\overline{u_p'^2}$ correlate with the increase in ℓ^+ , and so spatial filtering may be playing a role. Similar results were obtained by Morrison *et al.* (2004) in the SuperPipe for $1500 \leq Re_\tau \leq 10^5$, with $11.6 \leq \ell^+ \leq 385$, as shown in figure 5.

These experiments sparked a vigorous debate over the effects of spatial resolution. The data collected by Fernholz & Finley (1996) had suggested that $\ell^+ < 10$ was needed to measure $\overline{u_p'^2}$ accurately, while Hutchins *et al.* (2009) proposed the more restrictive criterion $\ell^+ < 4$. Since the non-dimensional Kolmogorov length scale $\eta^+ \approx 2$ near the wall (Yakhot, Bailey & Smits 2010), it appears that spatial filtering becomes important for $\ell > 2\eta$. What is more, spatial filtering effects continue to be important away from the wall. It seems intuitive, for example, that when ℓ^+ is comparable to y^+ , that is, when $y/\ell = O(1)$, spatial filtering is likely to be important. Thus the appearance of the outer peak may well be caused by the filtering of the signal at wall distances smaller than the outer peak location. For example, in figure 4 at $Re_\tau = 17\ 800$ ($Re_\theta = 57\ 720$) the outer peak is located at $y_o^+ \approx 500$ and $y/\ell \approx 7$, a point where spatial filtering might

Measurements in wall-bounded turbulence

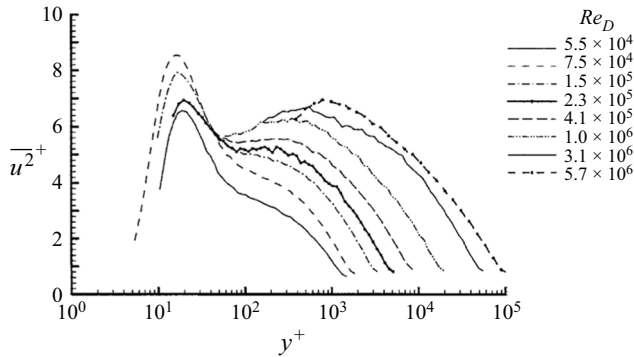


Figure 5. Streamwise turbulence intensity $\overline{u^2}^+$ in pipe flow for $Re_D = 5.5 \times 10^4$ – 5.7×10^6 ; $Re_\tau = 1500$ – $101\,000$, as measured in the Princeton SuperPipe. The corresponding values of ℓ^+ are 11.6 to 385. For the three highest Reynolds numbers, the outer peak is located at approximately $5\ell^+$. Figure adapted from Morrison *et al.* (2004) with permission.

still be important. For the highest Reynolds number studied by Morrison *et al.* (2004) ($Re_\tau = 10^5$), the corresponding numbers are $y_o^+ \approx 1000$ and $y/\ell \approx 3$. Hence the effects of spatial filtering can be pernicious, affecting our conclusions about the inner and outer peak, as well as the possible presence of a log law. These effects will be considered further below.

To help alleviate the errors associated with spatial filtering, a number of correction schemes have been put forward. A widely used method was proposed by Wyngaard (1968), and it is based, as many other methods are, on knowing the spectrum of the fluctuations and by assuming small-scale isotropy. In the near-wall region, however, the flow is strongly anisotropic, and the analysis by Cameron *et al.* (2010), based on a two-dimensional spectral representation, demonstrated the significant role of anisotropy in the spatial filtering behaviour of a hot wire. They also showed how the filtering can significantly affect the energy spectrum at wavenumbers much smaller than that corresponding to the wire length.

In a different approach, Smits *et al.* (2011) proposed a correction method based on eddy scaling. The method corrects for the effects of spatial resolution across the entire shear layer, and it appears to give accurate results over a wide range of wire lengths and flow Reynolds numbers. It was suggested that both ℓ^+ and y^+ are important so that, in functional form,

$$\overline{u^2}_T^+ = g(\ell^+, y^+) \overline{u^2}_m^+, \quad (5.2)$$

where $\overline{u^2}_T^+$ and $\overline{u^2}_m^+$ are the true and measured streamwise Reynolds stress, respectively. For a measurement at a single Reynolds number and a fixed wire length, ℓ^+ will be constant, and so a more particular functional form was proposed:

$$\overline{u^2}_T^+ = [1 + M(\ell^+)f(y^+)] \overline{u^2}_m^+. \quad (5.3)$$

That is, the function g can be separated into one part that depends on the wire length and another that depends on the wall distance. Because $M(\ell^+)$ is a constant for all values of y^+ , it only needs to be found at one location. If a measurement at $y^+ = 15$ is not available, a reasonable approximation is given by an empirical fit to selected numerical and experimental data so that

$$M(\ell^+) = 0.0091\ell^+ - 0.069, \quad (5.4)$$

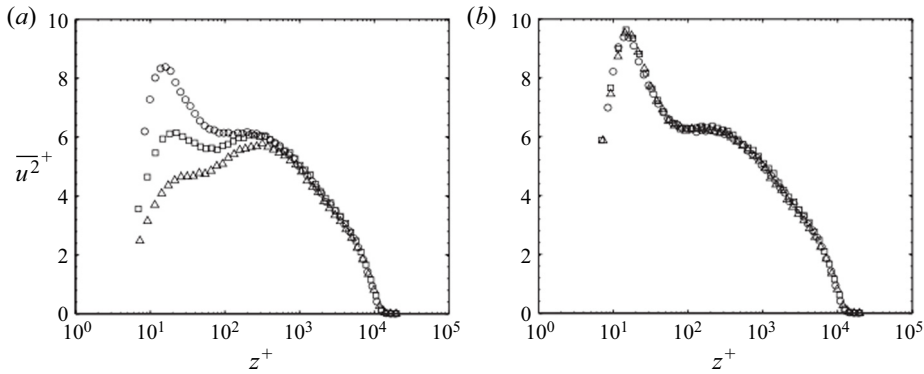


Figure 6. Streamwise Reynolds stress profiles measured in a turbulent boundary layer with various wire lengths at $Re_\tau = 13\,600$, $\circ \ell^+ = 22$, $\square \ell^+ = 79$ and $\triangle \ell^+ = 153$: (a) uncorrected data; (b) streamwise Reynolds stress profiles corrected using the correction proposed by Smits *et al.* (2011) using the measured value of $\overline{u_p^2}^+$ (the correction can provide this estimate and the results are similar). Data from Hutchins *et al.* (2009). Figure from Smits *et al.* (2011).

although this implies that a sensor length of $\ell^+ \leq 8$ will fully resolve the flow whereas in practice it seems that we need $\ell^+ \leq 4$.

The form of $f(y^+)$ was chosen according to three defining characteristics. First, in the viscous region, the Kolmogorov scale is the relevant scale, and since η^+ is nearly constant for $y^+ < 15$ we also expect the attenuation to be constant in this region. Second, f must be unity at $y^+ = 15$ because of the way the function $M(\ell^+)$ is estimated. Third, an ℓ/y dependence is likely, and so f is expected to vary as $1/y$ for $y^+ > 15$ in accordance with the attached eddy hypothesis. These features were incorporated into a suitable analytical function that obeyed these constraints while avoiding discontinuities; that is

$$f(y^+) = \frac{15 + \ln(2)}{y^+ + \ln[\exp^{(15-y^+)} + 1]}. \tag{5.5}$$

Equation (5.3) can then be used to correct the streamwise Reynolds stress measured using a finite length sensor to the value it would have if it had been acquired with an infinitesimally small one. This method works well for the data shown in figure 6, even for $\ell^+ = 153$. Its success appears to be due mostly to the fact that, outside the near-wall viscous region it uses the correct length scale, which is the distance from the wall rather than the viscous length scale. The figure also helps to illustrate the effects of spatial filtering on the apparent inner and outer peak behaviour: at this Reynolds number the outer peak is prominent in the uncorrected profiles but only nascent in the corrected profiles.

Equation (5.3) can also be used to evaluate the error in measuring $\overline{u^2}$. As shown in figure 7, the error decreases with the wall distance and increases with wire length. We see that for $\ell^+ \leq 100$, the error is always less than 3% for $y^+ > 5\ell^+$ and always less than 1.3% for $y^+ > 10\ell^+$.

What about LDV? In LDV the probe volume is approximately ellipsoidal with its long dimension oriented normal to the plane of measurement. The intersection of the two laser beams sets its length, and in the plane of measurement the volume has a circular cross-section of diameter d . Because each individual velocity realization in LDV corresponds to a single particle passing through the probe volume, in a statistically two-dimensional flow the probe volume length will have no significant effect on the turbulence statistics (Luchik & Tiederman 1985; Schultz & Flack 2013).

Measurements in wall-bounded turbulence

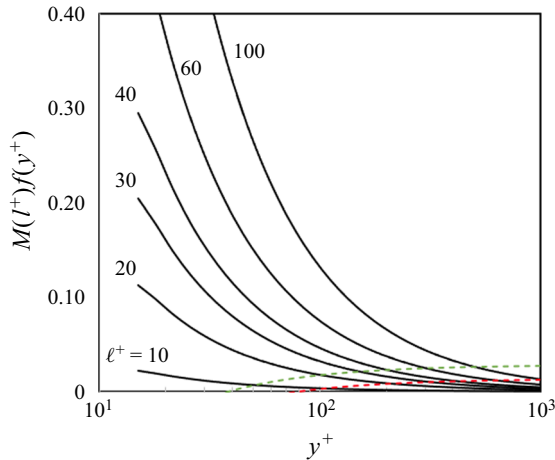


Figure 7. Estimate of the error due to spatial filtering as given by (5.3) as a function of ℓ^+ and y^+ . For $\ell^+ \leq 100$, the error in measuring u^2 is always less than 3% for $y^+ > 5\ell^+$ (green dashed line), and always less than 1.3% for $y^+ > 10\ell^+$ (red dashed line).

The critical parameter to characterize the spatial resolution is therefore the non-dimensional measurement volume diameter, d^+ , and a widely used correction scheme was proposed by Durst *et al.* (1998). However, their corrections for the second-order moments only accounted for variations in the mean velocity across the volume. But in the vicinity of the near-wall peak the turbulent stress gradients are severe, so they need to be taken into account. For example, if $d^+ = 10$, then at $y^+ = 15$ the measurement volume would span the peak in such a way as to reduce, by inspection from figure 6, the inferred turbulence level by approximately 3%. For $d^+ = 20$, this would be approximately 8%.

In this respect, De Graaff & Eaton (2000) used LDV with $d = 35 \mu\text{m}$ to study boundary layers at $539 \leq Re_\tau \leq 10\,070$. The data were taken in the Stanford high-pressure tunnel, and the results are shown in figure 8. The non-dimensional measurement volume diameter varied from $0.6 \leq d^+ \leq 10$, so that some level of spatial filtering might be expected in the near-wall region for the two highest Reynolds numbers. Also, given the scale of the experiment and the limitations of optical access, it was not possible to take data for $y^+ < 20$ at the highest Reynolds number. Nevertheless, this was a particularly important experiment, and we see a monotonic increase in $\overline{u_p^2}^+$ with Reynolds number, one of the first experiments to demonstrate this result. The outer peak is not evident, however, no doubt because the maximum Reynolds number was not high enough.

5.3. Nanoscale thermal anemometry probe

In an effort to improve the spatial resolution and frequency response of hot-wire anemometry, nanoscale thermal anemometry probes (NSTAP) were developed at Princeton (Kunkel, Arnold & Smits 2006; Bailey *et al.* 2010; Vallikivi *et al.* 2011; Vallikivi & Smits 2014). These probes were made using microelectromechanical systems techniques and yielded ribbon-shaped sensors with a typical width $w = 2 \mu\text{m}$, thickness $t = 0.1 \mu\text{m}$ and length ℓ of either 60 or 30 μm (see figure 9a). The sensors, therefore, have characteristic lengths approximately 10 times smaller than conventional hot wires, and as evident from figure 9(b) they also have a typical frequency response approximately 10 times higher. The square-wave results shown in this figure were supported by

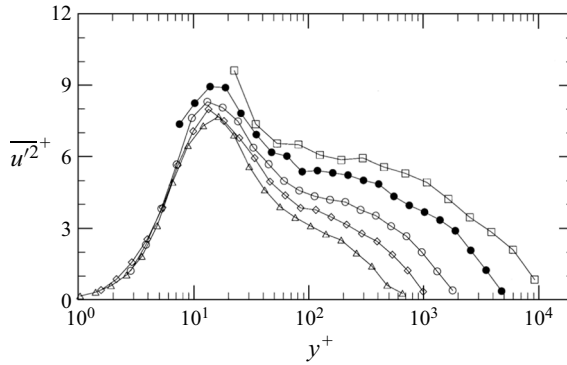


Figure 8. Streamwise turbulence intensity in boundary layers for $Re_\theta = 1430\text{--}31\,000$; $Re_\tau = 539, 993, 1708, 4238, 10\,070$. Data obtained using LDV with a measurement volume $35\ \mu\text{m}$ in diameter ($d^+ = 0.6$ to 10). Adapted from De Graaff & Eaton (2000) with permission.

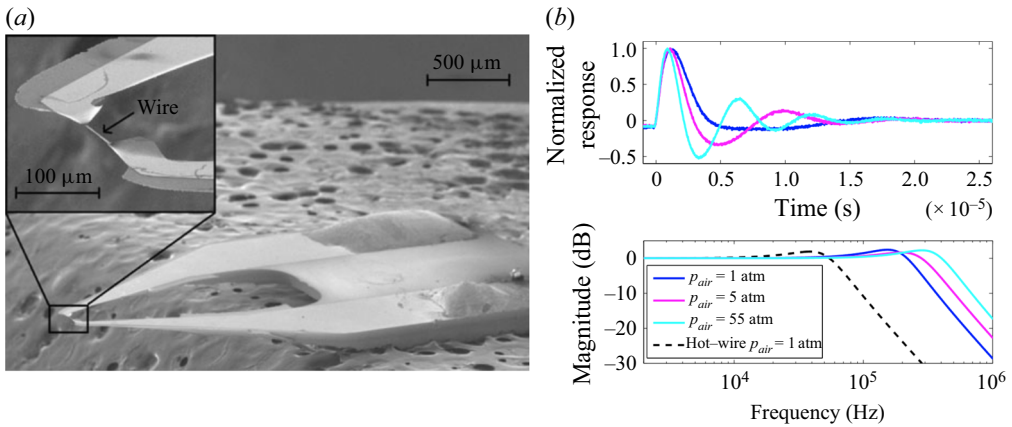


Figure 9. Configuration and performance of NSTAP ($\ell = 60\ \mu\text{m}$, $w = 1\ \mu\text{m}$, $t = 0.1\ \mu\text{m}$). (a) Scanning electron microscope images. The probe is mounted on a wax substrate (seen in the background) for imaging. From Vallikivi *et al.* (2011). (b) Temporal response of the NSTAP at different ambient air pressures. Top panel: square-wave response. Bottom panel: attenuation in signal with frequency (Bode diagram), where 0 dB indicates unity gain (estimated using square-wave response). From Vallikivi & Smits (2014) with permission.

Hutchins *et al.* (2015) in their experiments in the Princeton SuperPipe, where the response of a standard hot-wire probe ($\ell = 500\ \mu\text{m}$, $d = 2.5\ \mu\text{m}$) was compared with that of an NSTAP probe ($\ell = 60\ \mu\text{m}$, $w = 1\ \mu\text{m}$, $t = 0.1\ \mu\text{m}$). The results given in figure 10 confirm the superior response of the NSTAP at higher frequencies.

5.4. Log law for turbulence

NSTAP probes were used by Hultmark *et al.* (2012) in the SuperPipe at Reynolds numbers ranging from $Re_\tau = 1985$ to $98\,000$, with the corresponding value of ℓ^+ varying from 1.8 to 45.5. The results corrected according to (5.3) are shown in figure 11(a) in outer scaling and in figure 11(b) in inner scaling. Figure 11(a) plainly demonstrates the presence of a log law for turbulence over an extent that increases with Reynolds number. The solid line

Measurements in wall-bounded turbulence

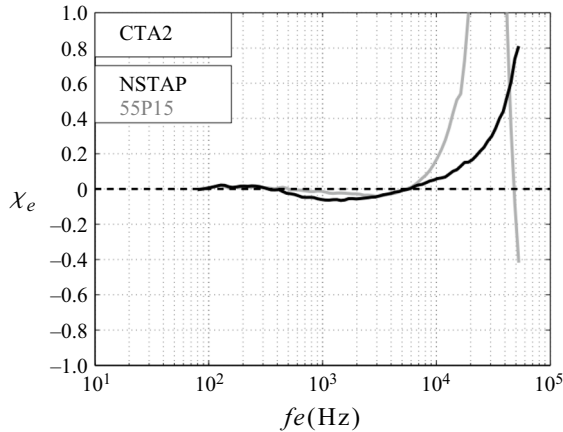


Figure 10. Comparison of the transfer function χ_e for the same anemometer, but different probes: (grey) standard probe CTA2 at $y^+ \approx 80$; (black) NSTAP at $y^+ \approx 29$ ($\tau_c = 3.7 \mu\text{s}$). Standard probe dimensions $\ell = 0.5 \text{ mm}$, $d = 2.5 \mu\text{m}$; NSTAP dimensions $\ell = 60 \mu\text{m}$, $w = 1 \mu\text{m}$, $t = 0.1 \mu\text{m}$. Here, χ_e is a difference function, defined as the fractional variation of the premultiplied spectra for a given experiment. From Hutchins *et al.* (2015) with permission.

is given by

$$\overline{u^2}^+ = B_1 - A_1 \ln(y/R), \quad (5.6)$$

with $A_1 = 1.25$ and $B_1 = 1.61$ ((4.2) with $V(y^+) = 0$). At the highest Reynolds number, the log law starts at approximately $0.01R$, where the errors due to spatial filtering are negligibly small ($< 0.5\%$). These measurements were the first to show unambiguously the presence of the log law in turbulence, which only became evident once $Re_\tau \geq 20 \times 10^3$. The extent of the log law increases with Reynolds number, and at the highest Reynolds number it spans more than 10% of the pipe radius. This experiment also found that the region over which the log law in turbulence applies coincides with the region of the log law in the mean velocity, a very satisfying observation from the point of view of our scaling arguments and the attached eddy hypothesis. Hultmark *et al.* (2012) suggested that the appearance of this extended logarithmic variation marks the onset of the extreme Reynolds number range for pipe flow. Hultmark *et al.* (2013) then showed that this same result applies to rough wall pipe flows, and Marusic *et al.* (2013) and Vallikivi, Hultmark & Smits (2015b) found that it additionally describes high Reynolds number boundary layers, where Marusic *et al.* suggested a slightly modified slope ($A_1 = 1.26$) and found that the additive constant depends on the flow: for pipes $B_1 = 1.56$, and for boundary layers $B_1 = 2.30$. They were the first to propose that A_1 be named the Townsend–Perry constant to mark their contributions to the underlying theory.

It should be noted that the argument for the log law in turbulence put forward by Perry & Abell (1977) and Perry *et al.* (1986) was based on a dimensional analysis of the energy spectra. For $\overline{u^2}$ and $\overline{w^2}$ they postulated two overlap regions in wavenumber space: one between the outer scaled eddies and the wall-attached eddies; and one between the wall-attached eddies and the dissipative eddies. The first overlap region yields a k^{-1} variation, and the second a $k^{-5/3}$ variation, where k is the streamwise wavenumber. These results are in line with ‘classical’ expectations, but high Reynolds number experiments at Princeton failed to confirm such trends (Morrison *et al.* 2002, 2004; Rosenberg *et al.* 2013; Vallikivi, Ganapathisubramani & Smits 2015a), as did the most recent measurements in

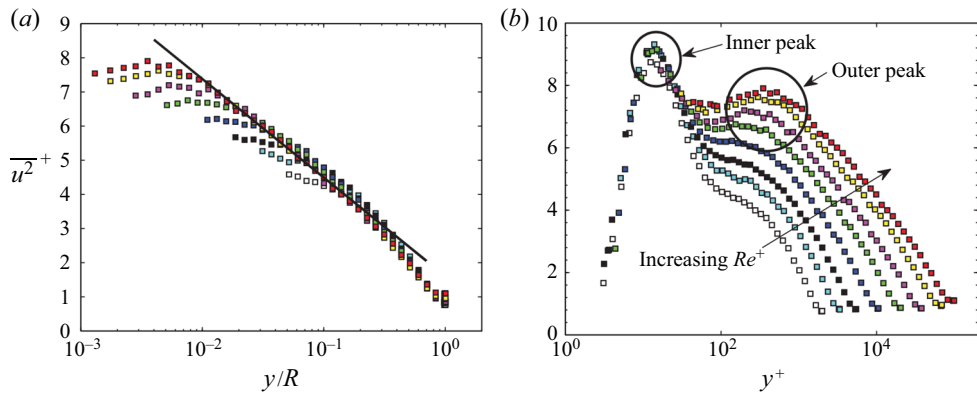


Figure 11. Streamwise turbulence intensity distributions for pipe flow. SuperPipe data for $Re_\tau = 1985$ to 98 200. Corrected according to (5.3) (Smits *et al.* 2011). The corresponding values of ℓ^+ varied from 1.8 to 45.5. (a) Profiles in outer layer scaling for $y^+ > 100$. The solid line is (5.6) with $A_1 = 1.25$ and $B_1 = 1.61$. (b) Profiles in inner layer scaling. For the four highest Reynolds numbers, the outer peak is located at a position $y^+ \geq 8\ell^+$. Adapted from Hultmark *et al.* (2012) with permission.

the Melbourne tunnel (Hwang, Hutchins & Marusic 2021). It appears that the existence of a well-developed k^{-1} spectrum is not a necessary condition for the presence of a logarithmic wall-normal dependence of the turbulence intensity. Hwang *et al.* (2021) also suggested, based on their analysis of the data, that the Townsend–Perry constant is weakly dependent on Reynolds number.

5.5. Inner and outer peaks

Consider now the SuperPipe results in inner scaling shown in figure 11(b). The first significant observation is with regard to the presence of the outer peak, which is clearly evident for $Re_\tau \geq 20\,000$. At the location of the outer peak ($y = y_o$) the correction for spatial filtering at the highest Reynolds number was approximately 2.4%, and at $y^+ = 0.5y_o$ the correction was approximately 3.1%, so that these observations on the appearance of an outer peak were the first that were not compromised by spatial filtering.

The second significant observation from figure 11(b) is with respect to the inner peak. As might be expected, despite using NSTAP probes, the inner peak could not be accurately resolved at the higher Reynolds numbers even when corrected according to (5.3). This is illustrated in figure 12, where the magnitude of the inner peak is compared with other data. The DNS data by Lee & Moser (2015) follow a logarithmic rise in the peak value, in agreement with previous work (Metzger *et al.* 2001; Marusic & Kunkel 2003), and they proposed that

$$\overline{u_p^2}^+ = a_1 + b_1 \ln(Re_\tau), \quad (5.7)$$

with $a_1 = 3.66$ and $b_1 = 0.642$. The hot-wire data taken in the Melbourne tunnel by Marusic *et al.* (2015) with $\ell^+ \approx 24$ is also shown, together with the same results corrected according to (5.3). The agreement of the corrected data with (5.7) is impressive, which might be taken as indirect support for the correction used here. For the lower Reynolds numbers the corrected SuperPipe data from Hultmark *et al.* (2012) agrees well with (5.3) but then diverges noticeably for $Re_\tau > 10\,000$. This is also true for the corrected HRTF boundary layer data by Vallikivi *et al.* (2015b), where the divergence occurs for $Re_\tau > 5000$. These trends are unlikely to be due to any uncertainty in the correction method, since for the NSTAP probes the correction for $Re_\tau < 40\,000$ was smaller than

Measurements in wall-bounded turbulence

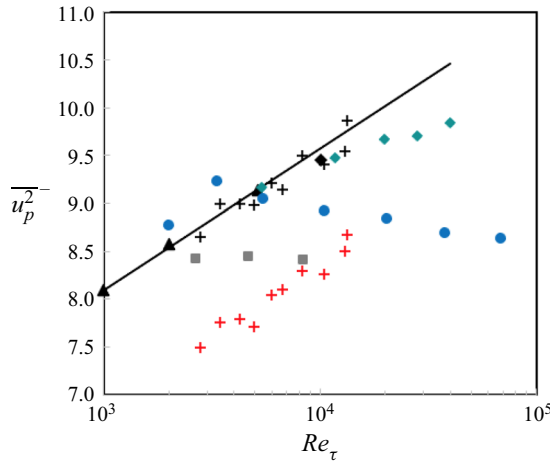


Figure 12. Reynolds number variation of inner peak magnitude. Data from Marusic *et al.* (2015) for matched $\ell^+ \approx 24$ (+, red); data from Marusic *et al.* (2015) corrected according to (5.3) (+); SuperPipe NSTAP data from Hultmark *et al.* (2012) (●, royal blue); HRTF NSTAP data from Vallikivi *et al.* (2015b) (■, grey); CICLoPE PIV data from Willert *et al.* (2017); ◊, channel flow DNS from Hoyas *et al.* (2022); △, channel flow DNS from Lee & Moser (2015); —, $u_p^2 = 3.66 + 0.642 \ln(Re_\tau)$ (proposed by Lee & Moser).

that applied to all of the Marusic *et al.* data. Monkewitz (2021) recently suggested that there could be some blockage effects caused by the NSTAP support system, and this may indeed be the case because for $Re_\tau \geq 10\,000$ the inner peak is very close to the wall (for the HRTF data $y_p < 0.1$ mm and $y_p/\ell < 1.66$). Finally, we see that the PIV data from the CICLoPE pipe flow facility (Willert *et al.* 2017) also shows some divergence at the higher Reynolds numbers, but this trend is likely due to spatial filtering, which was reported to be -7.5% at the highest Reynolds number.

In an effort to resolve these issues, NSTAPs were brought to the Melbourne wind tunnel, where the boundary layer is approximately 350 mm thick. The experiment therefore enabled unprecedented spatial resolution, so that even at the highest Reynolds number ($Re_\tau = 20\,000$) measurements could be made in the near-wall region while maintaining $\ell^+ < 3.5$. The profiles of $\overline{u^2}^+$ are shown in figure 13(a), and the inner peak magnitude indeed displayed the expected logarithmic variation with Reynolds number, as shown in figure 13(b). For the experimental and DNS data given in this figure, the variation is well represented by (5.7) with $a_1 = 3.54$ and $b_1 = 0.646$, very close to the values proposed by Lee & Moser (2015). This logarithmic growth in the inner peak magnitude remains to be verified at even higher Reynolds numbers, and recently Chen & Sreenivasan (2021) have argued that there must be a finite limit to its growth. This remains a topic for future investigation. Also, Smits *et al.* (2021) have proposed that the growth of the inner peak can be related to the wall stress fluctuations, which are influenced by the very large-scale motions in the outer flow (Marusic, Mathis & Hutchins 2010; Mathis *et al.* 2013; Agostini & Leschziner 2018; Marusic *et al.* 2021). On the basis of DNS data, Smits *et al.* concluded that only the contribution due to large-scale motions was Reynolds number dependent, and so the scaling in the near-wall region can be split into one function of y^+ and another for Re_τ ; that is, for $y^+ \leq 20$,

$$\overline{u^2}^+ = f_1(Re_\tau)f_2(y^+). \tag{5.8}$$

The outer limit for this scaling grows with Reynolds number, and the data by Samie *et al.* (2018) suggest that it reaches out to at least $y^+ \approx 50$ at $Re_\tau = 20\,000$.

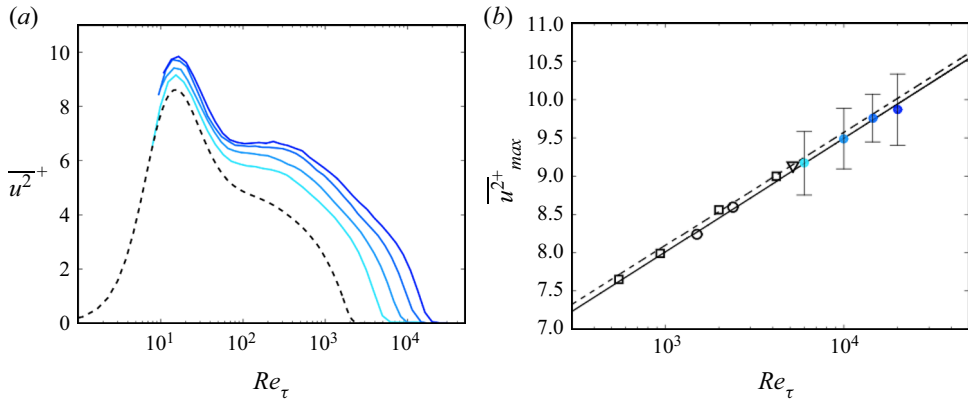


Figure 13. (a) Streamwise turbulence intensity in boundary layers for $Re_\tau = 6123, 10\,100, 14\,680, 19\,680$. Data obtained using NSTAP in the Melbourne wind tunnel with $\ell^+ = 2.5$ to 3.5 . (b) Dependence of inner peak magnitude on Reynolds number. Here: NSTAP (\bullet); DNS of turbulent boundary layer from Sillero, Jiménez & Moser (2013) (\circ); DNS of channel flow from Lozano-Durán & Jiménez (2014) (\square); DNS of channel flow from Lee & Moser (2015) (∇); $\overline{u^2}_p^+ = 3.54 + 0.646 \ln(Re_\tau)$ (—); $\overline{u^2}_p^+ = 3.66 + 0.642 \ln(Re_\tau)$ (---). From Samie *et al.* (2018) with permission.

5.6. Mesolayer

We have considered the attributes of the inner and outer peaks, but there is a region that lies between, often called the mesolayer, covering approximately the same region where the mean velocity profile is best described by a power law (3.1), that is, the region defined by $50 < y^+ < 300$. As noted by Vallikivi *et al.* (2015a), the concept of a mesolayer was initially introduced by Long & Chen (1981), and developed more fully by Afzal (1982), Afzal (1984), Sreenivasan & Sahay (1997), George & Castillo (1997), Wosnik, Castillo & George (2000) and Wei *et al.* (2005). Wei *et al.* (2005) described the mesolayer (layer III in their nomenclature) as a region where there is a balance between turbulent inertia (stress gradients), the viscous force and either the force due to the pressure gradient in pipes or the mean advection in boundary layers. With the exceptions of George & Castillo (1997) and Wosnik *et al.* (2000), these studies identify the mesolayer as a region where an intermediate wall-normal length scale emerges that increases as $\sqrt{Re_\tau}$, where this length scale is mostly identified with the location of the maximum in the shear stress (see, for example, Sreenivasan & Sahay 1997).

Vallikivi *et al.* (2015a) proposed bounds on the mesolayer that were different from those determined in previous studies. The lower bound was marked by the location where two peaks emerge in the premultiplied spectra, the ‘inner’ one corresponding to the large-scale motions and the ‘outer’ one corresponding to the very large-scale motions or superstructures ($y^+ > 50$ for the boundary layer and $y^+ > 67$ for the pipe). The energy associated with the outer spectral peak increases with distance from the wall, and its location acts as the outer bound for this region, which closely matches the start of the logarithmic regions in the mean flow and the variance. For the lower Reynolds numbers the location of the outer spectral peak appeared to follow the $\sqrt{Re_\tau}$ scaling proposed for pipes and boundary layers in previous studies, and where it closely tallies with the position of the maximum in the shear stress, but for $Re_\tau > 20\,000$ it went asymptotically to a more or less constant position (in viscous scaling).

Finally, it is interesting to note that the streamwise length scale associated with the outer spectral peak, inferred using Taylor’s hypothesis, appears as an intermediate length

Measurements in wall-bounded turbulence

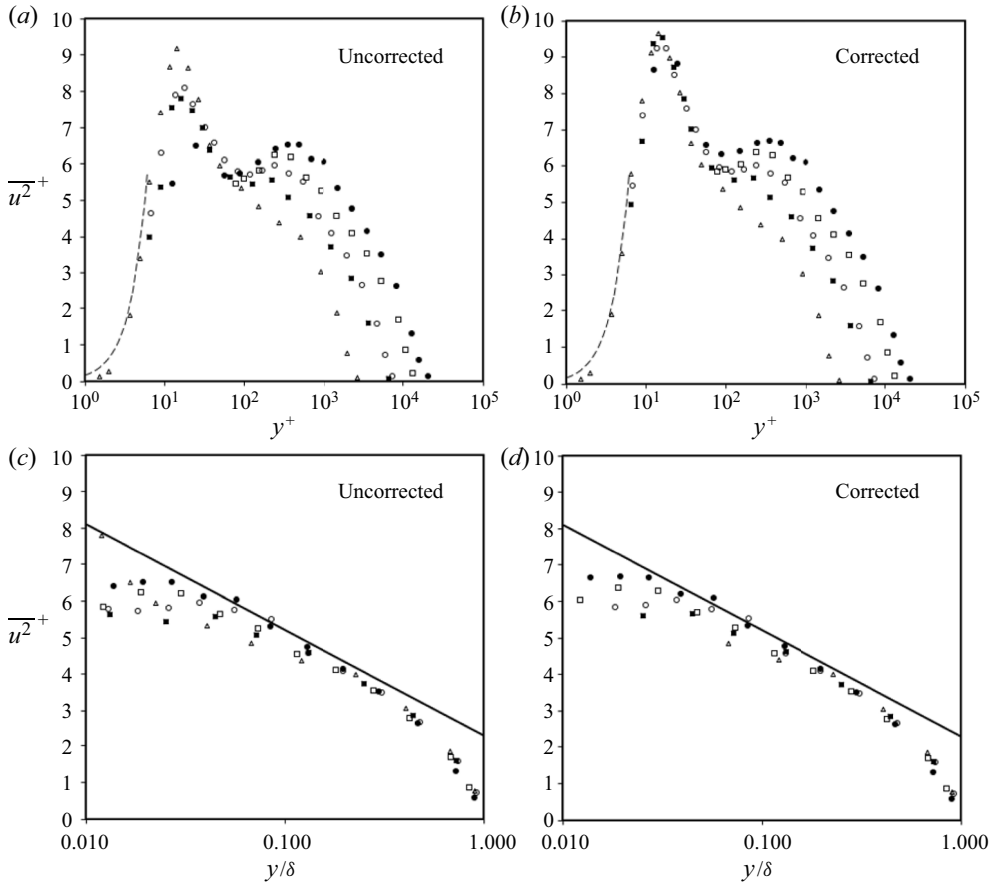


Figure 14. Boundary layer data from Fernholz & Finley (1996): (a,c) uncorrected; (b,d) corrected; (a,b) inner scaling; (c,d) outer scaling (for $y^+ > 100$ only). Symbols as in figure 4. The solid line is (5.6) with $A_1 = 1.26$ and $B_1 = 2.3$.

scale that seems to scale with $\sqrt{Re_\tau}$ in both pipes and boundary layers. Vallikivi *et al.* (2015a) therefore suggested that the mesolayer may be identified with the emergence of a new streamwise length scale rather than a new wall-normal length scale, as suggested previously.

5.7. Revisiting earlier data

With respect to the measurements by Fernholz & Finley (1996), given earlier in figure 4, we can now assess the effects of spatial filtering by correcting the data using (5.3). The comparison is shown in figure 14. The effects of spatial filtering are rather minor for $y^+ > 100$, and the outer peak remains clearly visible after the corrections are applied. Also, in the region where we would expect to see a logarithmic variation in u^2^+ the effects of spatial filtering are almost negligible, and the agreement with (5.6) is very good for the highest Reynolds numbers. It is apparent that this landmark experiment already contained the information necessary to establish the log law for turbulence and the development of the outer peak, but at the time it was unfortunately constrained by the absence of a suitable correction method for the effects of spatial filtering.

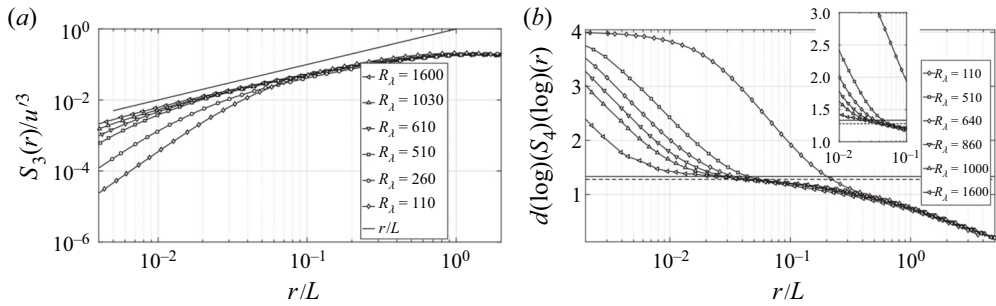


Figure 15. Measurements using NSTAP in the Göttingen Variable Density Turbulence Tunnel. (a) Third-order structure functions. Here, u' is the fluctuating velocity and L the integral length scale. The straight black line is equal to $r = L$, the scaling predicted by K41 4/5th law. (b) Logarithmic derivative of the fourth-order structure function with respect to the separation. Even at the highest Reynolds numbers measured, there seems to be only a slow approach to a horizontal line that would correspond to power-law scaling. The solid horizontal line is the prediction by K41 4/5th law, and the dashed line the prediction of the model by She & Leveque (1994). The inset shows an enlargement of the intersection region. From Sinhuber, Bewley & Bodenschatz (2017) with permission.

6. Future directions

6.1. Subminiature probe development

The development of NSTAP probes has obviously had a positive impact on our ability to measure turbulence at high Reynolds number. Le-The *et al.* (2021) have recently constructed a similar set of free-standing probes with $\ell = 70 \mu\text{m}$, $w \approx 300 \text{ nm}$ and $t \approx 100 \text{ nm}$, and Baradel *et al.* (2021) have fabricated comparable probes with $\ell = 60 \mu\text{m}$, $w \approx 200 \text{ nm}$ and $t \approx 1.5 \mu\text{m}$. We can therefore expect to see a growing use of such small probes in the coming years as they become more readily available. Here, we have reported their effectiveness in the context of measuring velocity fluctuations in wall-bounded flows, but they have also been successfully used in experiments on homogeneous isotropic turbulence in the Göttingen Variable Density Turbulence Tunnel, as shown in figure 15. With NSTAP, Taylor microscale Reynolds numbers up to 1600 were investigated. At the highest Reynolds number, the Kolmogorov scale η was $19 \mu\text{m}$ (Bodenschatz *et al.* 2014), so that the $30 \mu\text{m}$ NSTAP had $\ell/\eta < 1.6$, thereby avoiding any issues due to spatial filtering. The NSTAP probes have also been employed to investigate the atmospheric surface layer using constant current operation, and because of the high-frequency response of the probes no compensation was necessary (Huang *et al.* 2021). They have been used to quantify the errors due to finite probe size in grid turbulence (Ashok *et al.* 2012) and turbulent jets (Sadeghi, Lavoie & Pollard 2018), and to characterize the wake behind a horizontal-axis wind turbine at very high Reynolds numbers (Piqué, Miller & Hultmark 2020).

In addition, the NSTAP design has been extended to encompass a number of other applications (Fan *et al.* 2015). Two-component velocity measurements were made possible with the development of the X-NSTAP (Fu, Fan & Hultmark 2019; Byers *et al.* 2021), as illustrated in figure 16. Each of the crossed wires were of length $\ell = 60 \mu\text{m}$, and they were contained within a measurement volume measuring $42 \mu\text{m} \times 42 \mu\text{m} \times 50 \mu\text{m}$, which is comparable to the smallest NSTAP where $\ell = 30 \mu\text{m}$. Byers *et al.* (2021) used this probe to make two-component velocity measurements near the centreline of the SuperPipe for Reynolds numbers in the range $102 \leq Re_\lambda \leq 411$ ($1800 \leq Re_\tau \leq 24\,700$) to examine the inertial subrange scaling of the longitudinal and transverse velocity components. Even at the highest Reynolds number $\ell/\eta < 2.1$, so that spatial resolution issues were entirely avoided.

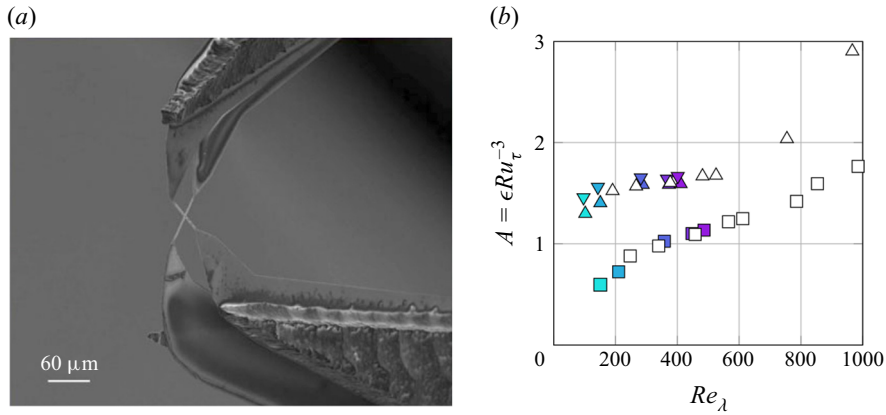


Figure 16. Configuration and performance of X-NSTAP. Measurement volume $42 \mu\text{m} \times 42 \mu\text{m} \times 50 \mu\text{m}$ ($\ell/\eta < 2.1$). (a) Scanning electron microscopy image of the X-NSTAP probe sensing elements. The two platinum sensing elements are shown perpendicular to each other to form an ‘X’. Each ribbon has $\ell = 60 \mu\text{m}$, $w = 1 \mu\text{m}$, $t = 0.1 \mu\text{m}$. The wires are separated by a $50 \mu\text{m}$ thick spacer. From Byers *et al.* (2021) with permission. (b) Non-dimensional dissipation rate on centreline of pipe flow. The symbols represent: the integration of longitudinal spectra (ϵ_u) (Δ); the integration of transverse spectra (ϵ_v) (∇); K41 4/5 law (\square). Filled symbols are results from the X-NSTAP measurements and hollow/white symbols represent the corresponding parameter from Morrison, Vallikivi & Smits (2016). From Byers *et al.* (2021) with permission.

6.2. Measuring temperature fluctuations

Another area of application for subminiature sensors is temperature measurement. A hot wire can be used to measure temperature fluctuations by operating it as a resistance thermometer, that is, by using a very small heating current, usually of order 1 mA. This ‘cold’ wire mode is not well-suited for constant temperature operation, and so the constant current mode is preferred. The primary issue is usually the frequency response. The NSTAP probes have a natural advantage in this respect because of their small thermal inertia, which typically improves the frequency response by an order of magnitude compared with conventional hot wires.

In a first step towards designing a cold-wire version of the NSTAP, Arwatz *et al.* (2013) devised a lumped-capacitance-based model to characterize the sensor dynamic response. The model consists of three parts corresponding to the wire filament, stubs and prongs, and it accounts for the interaction and heat transfer among these elements. The model can predict the response of the probe based on its physical properties and dimensions, and it demonstrated that end-conduction effects are often more severe than previously thought and that they can lead to significant errors in measuring temperature.

These lessons were applied by Arwatz *et al.* (2015) to develop an NSTAP probe specifically for temperature measurements, called T-NSTAP. The model had indicated that the probe performance could be improved in two specific ways. First, the thermal conductivity of the support structure was increased; instead of depositing a single platinum layer for the prongs, a 200 nm layer of gold was used because its thermal conductivity is more than four times higher. Second, the low-frequency response associated with end-conduction effects was improved by shortening the sensor support by 1 mm to reduce its thermal mass, and by increasing the length of the sensor to $200 \mu\text{m}$, approximately three times that of a regular NSTAP but still much shorter than conventional cold wires. Temperature measurements were then conducted in a heated grid-turbulence experiment with a cross-stream temperature gradient. The results given in figure 17(a) show that the

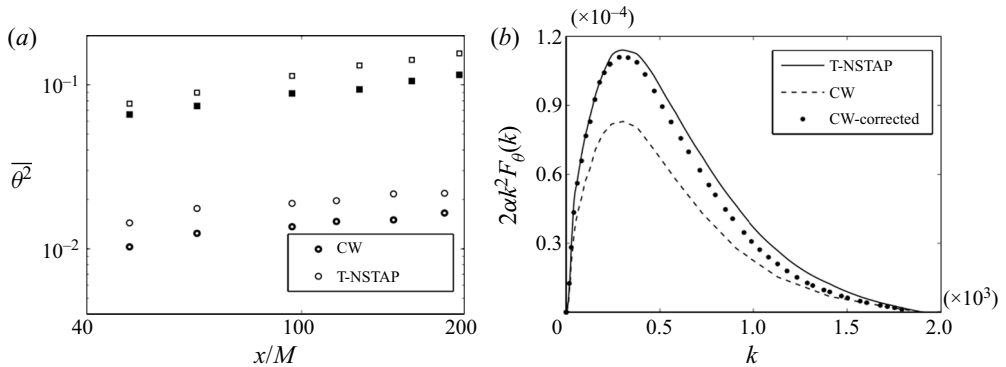


Figure 17. (a) Temperature variance for a cold wire and a T-NSTAP at 6 m s^{-1} (lower curves, circle symbol) and 9 m s^{-1} (higher curves, square symbol). Here x/M represents different cross-stream locations in a heated grid-turbulence set-up with a constant mean temperature gradient. From Arwatz *et al.* (2015) with permission. (b) One-dimensional temperature dissipation spectra measured using a cold wire and T-NSTAP. From Arwatz *et al.* (2015) with permission.

T-NSTAP is substantially more accurate in measuring the variances than a conventional cold wire, which can underestimate the temperature variance by up to 25 % and the rate of scalar dissipation by up to 35 %. By comparing the spectra, as in figure 17(b), we see that the improvement spans the entire frequency range. Furthermore, when the model was used to correct the cold-wire data, a convincing degree of agreement was achieved between the two sets of data. The T-NSTAP has also proved to be remarkably robust. In preliminary measurements of temperature fluctuations in the atmospheric surface layer, Arwatz mounted six T-NSTAPs on booms fixed to the airframe of an ultralight airplane. The ultralight took off, flew over Lake Geneva at a variety of altitudes and then landed, without breaking a single probe (Smits & Hultmark 2014).

In a further demonstration of the capabilities of T-NSTAP, Williams *et al.* (2015) made measurements of temperature in a rough-wall turbulent boundary layer subject to weakly stable stratification at the same time as measuring two components of velocity using PIV to determine heat fluxes. The T-NSTAP flat frequency response exceeded 300 Hz, so that no compensation of any kind was necessary, permitting accurate measurements of the temperature fluctuations, heat fluxes and temperature dissipation spectra.

Finally, NSTAP probes are being developed for supersonic flow (S-NSTAP), and promising results have been obtained using (compensated) constant current operation at Mach numbers up to 2, both at the Bundeswehr University in Munich (Kokmanian *et al.* 2019) and Aix Marseille Université (CNRS, IUSTI) in Marseille (Kokmanian *et al.* 2021).

6.3. PIV and spatial resolution

In the context of high-resolution, high-accuracy measurement of turbulence, we have largely neglected any discussion of the role of PIV. Probably the most significant challenge to its success in this area is finding a way to use PIV so that the large- and the small-scale motions can be resolved at the same time. This conundrum was succinctly stated by Lavoie *et al.* (2007). ‘The relatively coarse resolution of the PIV is somewhat typical of this measurement technique, where the scale resolution is a trade-off between zooming the image onto a small area to resolve small-scale motion, which can lead to a loss of global information and increases noise . . . , and capturing the region of the flow field that includes

all relevant scales . . .'. In this respect, Adrian (1997) defined the dynamic spatial range of PIV as the field-of-view in the object space divided by the smallest resolvable spatial variation, so that a system with a large dynamic spatial resolution allows measurements of small-scale velocity variations embedded in larger-scale motions. It is clear that the limit on resolving the largest motions is set by the size of the field-of-view, and this limit is well understood. As to the limit on resolving the smallest scales in PIV, it is set by a combination of the thickness of the illuminating sheet and the size of the interrogation window, where the latter is generally a compromise between spatial resolution and data quality requirements in that smaller windows increase the number of spurious velocity vectors due to a reduction in the number of particles for each window (Lavoie *et al.* 2007).

To quantify and correct for the finite spatial resolution of PIV measurements, Lavoie *et al.* (2007) developed an analytical method similar to the approach used by Wyngaard (1968) for hot-wire anemometry. Their analysis was restricted to measurements in homogeneous isotropic turbulence, so the effects of spatial gradients were not considered. The main drawback of their approach, shared by Wyngaard's method, is that to correct any one component the spectrum for that component needs to be known. Since this almost always requires a matching hot-wire measurement, the method is restricted in its utility. Nevertheless, they noted that, for their case, the filtering effect of PIV on the spectrum for $k_1 \eta > 0.5$ was similar to a hot wire with $\ell = 2W$, where W was the final (square) interrogation window size, so that the effects of spatial filtering in PIV in homogeneous isotropic turbulence is apparently more severe than that for hot wires. Unfortunately, this conclusion is difficult to translate to applications in wall-bounded flows. For example, in the usual set-up for measuring $\overline{u^2}$ the PIV window is oriented in the streamwise plane, whereas the hot wire would be oriented in the spanwise direction.

A good example of how the spatial resolution of PIV in wall-bounded flows might be estimated is given by the experiment by Willert *et al.* (2017) in the CICLoPE pipe flow. Here, the missing energy due to PIV filtering was estimated using the one-dimensional transfer function of PIV for the streamwise spectrum proposed by Foucaut, Carlier & Stanislas (2004), and applying this estimate to the hot-wire spectrum of a boundary layer obtained by Carlier & Stanislas (2005). The difference between the integral of the filtered spectrum and that of the original spectrum was proposed as the best estimate of the missing energy. In fact, this approach is not so different from that used by Lavoie *et al.* (2007), in that it also requires independent information on the spectral content of the signal.

These considerations address the estimates of the streamwise component, but one of the persistent problems with PIV is that the wall-normal and shear Reynolds stresses are often underestimated, even when the streamwise component is well resolved. This is most evident in high-speed, compressible flows (Williams 2014; Williams *et al.* 2018), but it has been observed at all Mach numbers (see, for example, Bross, Scharnowski & Kähler 2021). Recently, Aultman, Disotell & Duan (2022) used DNS to investigate the spatial resolution of PIV for the wall-normal components and clearly demonstrated the important role played by window size, and how spurious cross-correlations caused by the size of the illumination diameter and the local particle density set limits on the smallest acceptable window size.

7. Summary and concluding remarks

I hope to have shown that our current understanding of turbulent wall-bounded flows has been enabled by major advances in measurement techniques. Hot-wire anemometry, LDV and PIV have all contributed, often in a complementary manner. One of the

major obstacles to progress in the past had been the filtering due to limited spatial resolution, which gave rise to well-founded doubts on some newly discovered features of high Reynolds number turbulence. Determining the inner and outer peak behaviour, and establishing the presence of the log law in turbulence, all depend crucially on either eliminating all spatial filtering, or keeping the filtering effects sufficiently small so that they can be convincingly corrected.

In hot-wire anemometry, the development of NSTAP, combined with the advent of purpose-built high Reynolds number facilities and a deeper understanding of spatial filtering, has now firmly established the log law in $\overline{u^{2+}}$ over approximately the same physical extent occupied by the log law in the mean velocity. We have also seen evidence for the log law in $\overline{w^{2+}}$. This was first noted in the channel flow DNS data of Lee & Moser (2015), and then experimentally verified at higher Reynolds numbers by Zimmerman *et al.* (2019) and Baidya *et al.* (2021). The latter data were obtained in the Melbourne tunnel for Re_τ up to 18 400, and with respect to (4.3) they found $A_2 \approx 0.27$ with B_2 displaying a slow logarithmic increase with Reynolds number.

In addition to the log law in turbulence, experiments have now verified the presence of an outer peak in $\overline{u^{2+}}$ at high Reynolds numbers in pipe and boundary layer flows, and unambiguously demonstrated the logarithmic growth in the inner peak with Reynolds number, at least for Re_τ up to approximately 20 000.

When the effects of spatial filtering cannot be avoided entirely, it seems that the method proposed by Smits *et al.* (2011) gives reasonable results for $\ell^+ \leq 70$ and $y^+/\ell^+ \geq 3$. Given this tool, it was possible to revisit the hot-wire data obtained in the DNW by Fernholz & Finley (1996). For $y^+ > 100$ the corrected data agreed in almost every respect with the NSTAP data obtained in the SuperPipe by Hultmark, Bailey & Smits (2010) and Hultmark *et al.* (2012), and in the boundary layer tunnel at Melbourne University by Samie *et al.* (2018). Therefore, the DNW experiments appear to be the first to establish the presence of the outer peak and the log law in turbulence. Unfortunately, they were not recognized as such at the time, primarily because of doubts regarding the effects of spatial filtering.

One of the more surprising conclusions from our survey of turbulence measurements is that experiments on the mean flow are simply not accurate enough to evaluate von Kármán's constant to better than 0.40 ± 0.02 . In addition, the inner peak in the streamwise turbulence increases logarithmically with Re_τ , but at a rate that is considerably slower than expected from the attached-eddy model, and the origin of the outer peak remains to be explained (Smits 2020). Also, spectral data on the streamwise velocity fluctuation point to the elusiveness of the asymptotic behaviour with increasing Reynolds number. For example, the slope of the inertial region asymptotes very slowly to $k^{-5/3}$, and no k^{-1} region was found at the Reynolds numbers reported here. Furthermore, there is a pressing need for additional high Reynolds number experiments to examine more fully the behaviour of the other turbulence components that include measurements of spectra and higher-order moments, to build on the work by, for example, Meneveau & Marusic (2013) and Baidya *et al.* (2021). Beyond isothermal flows, there is wide scope for new work to investigate flows with heat transfer where we know that the analogies between momentum and scalar transport are notably fragile.

New high Reynolds number experiments and computations are undoubtedly necessary to resolve these questions, as well as many others. It will be especially interesting to examine flow-specific trends by comparing pipe, channel and boundary layer behaviour. We have seen that high Reynolds number experiments in pipe and boundary layer flows are now routine, supported to a great extent by advanced measurement techniques. For many practical reasons, however, it seems unlikely that we will see comparable experiments

Measurements in wall-bounded turbulence

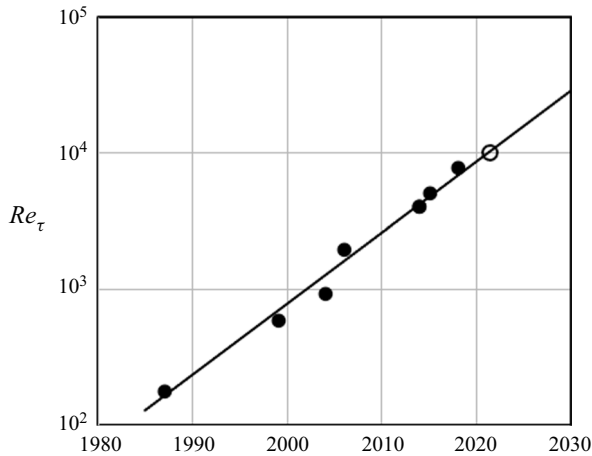


Figure 18. A log–linear plot of Reynolds number achieved in DNS of channel flow (Kim, Moin & Moser 1987; Moser, Kim & Mansour 1999; del Álamo *et al.* 2004; Hoyas & Jiménez 2006; Bernardini, Pirozzoli & Orlandi 2014; Lozano-Durán & Jiménez 2014; Lee & Moser 2015; Yamamoto & Tsuji 2018; Oberlack *et al.* 2022).

on high Reynolds number channel flows. As to DNS, high Reynolds number boundary layer computations will be very expensive, but for channel and pipe flows the limits on Reynolds number are being pushed aggressively. For example, recent DNS of channel flow at $Re^+ = 8000$ and 10 000 found a small region of log law in both the mean velocity and $\overline{u^{2+}}$ (Yamamoto & Tsuji 2018; Hoyas *et al.* 2022), and higher Reynolds numbers will soon be available. Figure 18 shows that for channel flow DNS the increase in Reynolds number is almost exactly logarithmic in time. In addition, recent DNS of pipe flow has reached Reynolds numbers of 5200 (Yao *et al.* 2021) and 6000 (Pirozzoli *et al.* 2021). Given this broadening scope of experiments and computations, the future looks exciting indeed.

Acknowledgements. Professors I. Marusic, M. Hultmark, J. Morrison and Dr L. Ding kindly provided comments on an earlier draft.

Funding. This work was supported by ONR under grants N00014-17-1-2309 and N00014-19-1-2301 (Program Manager P. Chang), and N00014-1-1-0533 (Program Manager R. Brizzolera).

Declaration of interests. The author reports no conflict of interest.

Author ORCIDs.

 Alexander J. Smits <https://orcid.org/0000-0002-3883-8648>.

REFERENCES

- ADRIAN, R.J. 1984 Scattering particle characteristics and their effect on pulsed laser measurements of fluid flow: speckle velocimetry vs particle image velocimetry. *Appl. Opt.* **23** (11), 1690–1691.
- ADRIAN, R.J. 1997 Dynamic ranges of velocity and spatial resolution of particle image velocimetry. *Meas. Sci. Tech.* **8** (12), 1393.
- ADRIAN, R.J. & GOLDSTEIN, R.J. 1971 Analysis of a laser Doppler anemometer. *J. Phys. E: Sci. Instrum.* **4** (7), 505.
- ADRIAN, R.J. & WESTERWEEL, J. 2011 *Particle Image Velocimetry*. Cambridge University Press.
- AFZAL, N. 1982 Fully developed turbulent flow in a pipe: an intermediate layer. *Ing. Arch.* **52**, 355–377.
- AFZAL, N. 1984 Mesolayer theory for turbulent flows. *AIAA J.* **22**, 437–439.

- AGOSTINI, L. & LESCHZINER, M. 2018 The impact of footprints of large-scale outer structures on the near-wall layer in the presence of drag-reducing spanwise wall motion. *Flow Turbul. Combust.* **100** (4), 1037–1061.
- DEL ÁLAMO, J.C., JIMÉNEZ, J., ZANDONADE, P. & MOSER, R.D. 2004 Scaling of the energy spectra of turbulent channels. *J. Fluid Mech.* **500**, 135–144.
- ARWATZ, G., BAHRI, C., SMITS, A.J. & HULTMARK, M. 2013 Dynamic calibration and modeling of a cold wire for temperature measurement. *Meas. Sci. Tech.* **24** (12), 125301.
- ARWATZ, G., FAN, Y., BAHRI, C. & HULTMARK, M. 2015 Development and characterization of a nano-scale temperature sensor (T-NSTAP) for turbulent temperature measurements. *Meas. Sci. Tech.* **26** (3), 035103.
- ASHOK, A., BAILEY, S.C.C., HULTMARK, M. & SMITS, A.J. 2012 Hot-wire spatial resolution effects in measurements of grid-generated turbulence. *Exp. Fluids* **53** (6), 1713–1722.
- AULTMAN, M.T., DISOTELL, K. & DUAN, L. 2022 The effect of particle lag on statistics of hypersonic turbulent boundary layers subject to pressure gradients. *AIAA Paper* 2022-1062.
- BAIDYA, R., PHILIP, J., HUTCHINS, N., MONTY, J.P. & MARUSIC, I. 2021 Spanwise velocity statistics in high-Reynolds-number turbulent boundary layers. *J. Fluid Mech.* **913**, A35.
- BAILEY, S.C.C., *et al.* 2013 Obtaining accurate mean velocity measurements in high Reynolds number turbulent boundary layers using Pitot tubes. *J. Fluid Mech.* **715**, 642–670.
- BAILEY, S.C.C., KUNKEL, G.J., HULTMARK, M., VALLIKIVI, M., HILL, J.P., MEYER, K.A., TSAY, C., ARNOLD, C.B. & SMITS, A.J. 2010 Turbulence measurements using a nanoscale thermal anemometry probe. *J. Fluid Mech.* **663**, 160–179.
- BAILEY, S.C.C., VALLIKIVI, M., HULTMARK, M. & SMITS, A.J. 2014 Estimating the value of von Kármán's constant in turbulent pipe flow. *J. Fluid Mech.* **749**, 79–98.
- BARADEL, B., LEON, O., GIANI, A., COMBETTE, P. & MERY, F. 2021 Micro thermal anemometer (μ TA) for turbulence measurement: development, fabrication and characterization. In *2021 Symposium on Design, Test, Integration & Packaging of MEMS and MOEMS (DTIP)*, pp. 1–6. IEEE.
- BARRE, S., DUPONT, P., ARZOUMANIAN, E., DUSSAUGE, J.P. & DEBIEVE, J.F. 1993 Some recent developments in constant current hot-wire anemometry of turbulent supersonic flows. In *Advances in Applied Mechanics* (ed. D.E. Stock, S.A. Sherif, A.J. Smits & J. Davidson), vol. ASME FED 167, pp. 199–208. ASME.
- BERNARDINI, M., PIROZZOLI, S. & ORLANDI, P. 2014 Velocity statistics in turbulent channel flow up to $Re_\tau \approx 4000$. *J. Fluid Mech.* **742**, 171–191.
- BESTION, D., GAVIGLIO, J. & BONNET, J.P. 1983 Comparison between constant-current and constant-temperature hot-wire anemometers in high-speed flows. *Rev. Sci. Instrum.* **54** (11), 1513–1524.
- BODENSCHATZ, E., BEWLEY, G.P., NOBACH, H., SINHUBER, M. & XU, H. 2014 Variable density turbulence tunnel facility. *Rev. Sci. Instrum.* **85** (9), 093908.
- BRIASSULIS, G., HONKAN, A., ANDREOPOULOS, J. & WATKINS, C.B. 1995 Application of hot-wire anemometry in shock-tube flows. *Exp. Fluids* **19** (1), 29–37.
- BROSS, M., SCHARNOWSKI, S. & KÄHLER, C.J. 2021 Large-scale coherent structures in compressible turbulent boundary layers. *J. Fluid Mech.* **911**, A2.
- BRUNS, J., DENGEL, P. & FERNHOLZ, H.H. 1992 Mean flow and turbulence measurements in an incompressible two-dimensional turbulent boundary layer. Part I: data. Institutsbericht Nr. 02/92, Hermann-Föttinger-Institut für Thermo- und Fluidodynamik, Technische Universität Berlin.
- BRUUN, H.H. 1995 *Hot-Wire Anemometry: Principles and Signal Analysis*. Oxford University Press.
- BYERS, C.P., HULTMARK, M., MARUSIC, I. & FU, M.K. 2021 Examining the inertial subrange with nanoscale cross-wire measurements of turbulent pipe flow at high Reynolds number near the centreline. *J. Fluid Mech.* **919**, A21.
- CAMERON, J.D., MORRIS, S.C., BAILEY, S.C.C. & SMITS, A.J. 2010 Effects of hot-wire length on the measurement of turbulent spectra in anisotropic flows. *Meas. Sci. Technol.* **21** (10), 105407.
- CARLIER, J. & STANISLAS, M. 2005 Experimental study of eddy structures in a turbulent boundary layer using particle image velocimetry. *J. Fluid Mech.* **535**, 143–188.
- CHEN, X. & SREENIVASAN, K.R. 2021 Reynolds number scaling of the peak turbulence intensity in wall flows. *J. Fluid Mech.* **908**, R3.
- COMTE-BELLOT, G. 1976 Hot-wire anemometry. *Ann. Rev. Fluid Mech.* **8**, 209–231.
- DE BREDERODE, V. & BRADSHAW, P.B. 1974 A note on the empirical constants appearing in the logarithmic law for turbulent wall flows. I. C. Aero. Rep. 74-43. Aeronautics Department, Imperial College, London.
- DE GRAAFF, D.B. & EATON, J.K. 2000 Reynolds-number scaling of the flat-plate turbulent boundary layer. *J. Fluid Mech.* **422**, 319–346.
- DRYDEN, H.L. & KUETHE, A.M. 1929 The measurement of fluctuations of air speed by the hot-wire anemometer. *NACA Report* 320.

- DUNCAN, W.J., THOM, A.S. & YOUNG, A.D. 1970 *Mechanics of Fluids*, 2nd edn. Edward Arnold.
- DURST, F., FISCHER, M., JOVANOVIĆ, J. & KIKURA, H. 1998 Methods to set up and investigate low Reynolds number, fully developed turbulent plane channel flows. *Trans. ASME J. Fluids Engng* **120**, 496–503.
- DURST, F., MELLING, A. & WHITELAW, J.H. 1976 *Principles and Practice of Laser-Doppler Anemometry*. Academic Press.
- FAN, Y., ARWATZ, G., VAN BUREN, T., HOFFMAN, D.E. & HULTMARK, M. 2015 Nanoscale sensing devices for turbulence measurements. *Exp. Fluids* **56** (7), 138.
- FERNHOLZ, H.H. & FINLEY, P.J. 1996 The incompressible zero-pressure-gradient turbulent boundary layer: an assessment of the data. *Prog. Aerospace Sci.* **32**, 245–311.
- FERNHOLZ, H.H., KRAUSE, E., NOCKEMANN, M. & SCHOBER, M. 1995 Comparative measurements in the canonical boundary layer at $Re_{\delta_2} \leq 6 \times 10^4$ on the wall of the German–Dutch wind tunnel. *Phys. Fluids* **7** (6), 1275–1281.
- FINGERSON, L.M. 1994 Thermal anemometry, current state, and future directions. *Rev. Sci. Instrum.* **65** (2), 285–300.
- FOUCAUT, J.-M., CARLIER, J. & STANISLAS, M. 2004 PIV optimization for the study of turbulent flow using spectral analysis. *Meas. Sci. Tech.* **15** (6), 1046.
- FRANKLIN, R.E. & WALLACE, J.M. 1970 Absolute measurements of static-hole error using flush transducers. *J. Fluid Mech.* **42**, 33–48.
- FREYMUTH, P. 1978 A bibliography of thermal anemometry. *TSI Quart.* **4** (4), 26.
- FU, M.K., FAN, Y. & HULTMARK, M. 2019 Design and validation of a nanoscale cross-wire probe (X-NSTAP). *Exp. Fluids* **60** (6), 99.
- FURUICHI, N., TERAOKA, Y. & TSUJI, Y. 2017 High Reynolds number experimental facilities for turbulent pipe flow at NMIJ. In *Progress in Turbulence VII*, pp. 95–100. Springer.
- FURUICHI, N., TERAOKA, Y., WADA, Y. & TSUJI, Y. 2018 Further experiments for mean velocity profile of pipe flow at high Reynolds number. *Phys. Fluids* **30** (5), 055101.
- GEORGE, W.K. & CASTILLO, L. 1997 Zero-pressure-gradient turbulent boundary layer. *Appl. Mech. Rev.* **50**, 689–729.
- GEORGE, W.K. & LUMLEY, J.L. 1973 The laser-Doppler velocimeter and its application to the measurement of turbulence. *J. Fluid Mech.* **60** (2), 321–362.
- HOYAS, S. & JIMÉNEZ, J. 2006 Scaling of the velocity fluctuations in turbulent channels up to $Re_{\tau} = 2003$. *Phys. Fluids* **18**, 011702.
- HOYAS, S., OBERLACK, M., ALCÁNTARA-ÁVILA, F., KRAHEBERGER, S.V. & LAUX, J. 2022 Wall turbulence at high friction Reynolds numbers. *Phys. Rev. Fluids* **7**, 014602.
- HUANG, K.Y., BRUNNER, C.E., FU, M.K., KOKMANIAN, K., MORRISON, T.J., PERELET, A.O., CALAF, M., PARDYJAK, E. & HULTMARK, M. 2021 Investigation of the atmospheric surface layer using a novel high-resolution sensor array. *Exp. Fluids* **62** (4), 76.
- HULTMARK, M., ASHOK, A. & SMITS, A.J. 2011 A new criterion for end-conduction effects in hot-wire anemometry. *Meas. Sci. Tech.* **22** (5), 055401.
- HULTMARK, M., BAILEY, S.C.C. & SMITS, A.J. 2010 Scaling of near-wall turbulence in pipe flow. *J. Fluid Mech.* **649**, 103–113.
- HULTMARK, M., VALLIKIVI, M., BAILEY, S.C.C. & SMITS, A.J. 2012 Turbulent pipe flow at extreme Reynolds numbers. *Phys. Rev. Lett.* **108** (9), 094501.
- HULTMARK, M., VALLIKIVI, M., BAILEY, S.C.C. & SMITS, A.J. 2013 Logarithmic scaling of turbulence in smooth- and rough-wall pipe flow. *J. Fluid Mech.* **728**, 376–395.
- HUTCHINS, N., MONTY, J.P., HULTMARK, M. & SMITS, A.J. 2015 A direct measure of the frequency response of hot-wire anemometers: temporal resolution issues in wall-bounded turbulence. *Exp. Fluids* **56** (1), 18.
- HUTCHINS, N., NICKELS, T.B., MARUSIC, I. & CHONG, M.S. 2009 Hot-wire spatial resolution issues in wall-bounded turbulence. *J. Fluid Mech.* **635** (-1), 103–136.
- HWANG, Y., HUTCHINS, N. & MARUSIC, I. 2021 The logarithmic variance of streamwise velocity and k–1 conundrum in wall turbulence. *J. Fluid Mech.* **933**, A8.
- JIMÉNEZ, J.M., HULTMARK, M. & SMITS, A.J. 2010 The intermediate wake of a body of revolution at high Reynolds numbers. *J. Fluid Mech.* **659**, 516–539.
- JOHNSTONE, R., COLEMAN, G.N. & SPALART, P.R. 2010 The resilience of the logarithmic law to pressure gradients: evidence from direct numerical simulation. *J. Fluid Mech.* **643**, 163–175.
- VON KÁRMÁN, T. 1930 Mechanische Ähnlichkeit und Turbulenz. In *Proceedings of the 3rd International Congress on Applied Mechanics, Part I*, 85.
- KIM, J., MOIN, P. & MOSER, R.D. 1987 Turbulence statistics in fully developed channel flow at low Reynolds number. *J. Fluid Mech.* **177**, 133–166.

- KING, L.V. 1914 On the convection of heat from small cylinders in a stream of fluid: determination of the convection constants of small platinum wires with applications to hot-wire anemometry. *Phil. Trans. R. Soc. Lond. A* **214** (509-522), 373–432.
- KOKMANIAN, K., BARROS, D.C., HULTMARK, M. & DUPONT, P. 2021 Heat transfer measurements of a nanoscale hot-wire in supersonic flow. *Exp. Fluids* **62** (8), 171.
- KOKMANIAN, K., SCHARNOWSKI, S., BROSS, M., DUVVURI, S., FU, M.K., KÄHLER, C.J. & HULTMARK, M. 2019 Development of a nanoscale hot-wire probe for supersonic flow applications. *Exp. Fluids* **60** (10), 1–10.
- KUNKEL, G., ARNOLD, C.B. & SMITS, A.J. 2006 Development of NSTAP: nanoscale thermal anemometry probe. *AIAA Paper* 2006-3718.
- LAVOIE, P., AVALLONE, G., DE GREGORIO, F., ROMANO, G.P. & ANTONIA, R.A. 2007 Spatial resolution of PIV for the measurement of turbulence. *Exp. Fluids* **43** (1), 39–51.
- LE-THE, H., KÜCHLER, C., VAN DEN BERG, A., BODENSCHATZ, E., LOHSE, D. & KRUG, D. 2021 Fabrication of freestanding Pt nanowires for use as thermal anemometry probes in turbulence measurements. *Microsyst. Nanoeng.* **7** (1), 28.
- LEE, M. & MOSER, R.D. 2015 Direct numerical simulation of turbulent channel flow up to $Re_\tau \approx 5200$. *J. Fluid Mech.* **774**, 395–415.
- LEE, T., NONOMURA, T., ASAI, K. & NAUGHTON, J.W. 2019 Validation and uncertainty analysis of global luminescent oil-film skin-friction field measurement. *Meas. Sci. Tech.* **31** (3), 035204.
- LIGRANI, P.M. & BRADSHAW, P. 1987 Subminiature hot-wire sensors: development and use. *J. Phys. E: Sci. Instrum.* **20**, 323–332.
- LOMAS, C.G. 1986 *Fundamentals of Hot-Wire Anemometry*. Cambridge University Press.
- LONG, R.R. & CHEN, T. 1981 Experimental evidence for the existence of the ‘mesolayer’ in turbulent systems. *J. Fluid Mech.* **105**, 9–59.
- LOZANO-DURÁN, A. & JIMÉNEZ, J. 2014 Effect of the computational domain on direct simulations of turbulent channels up to $Re_\tau = 4200$. *Phys. Fluids* **26**, 011702.
- LUCHIK, T.S. & TIEDERMAN, W.G. 1985 Effect of spanwise probe volume length on laser velocimeter measurements in wall bounded turbulent flows. *Exp. Fluids* **3** (6), 339–341.
- MACMILLAN, F.A. 1954 Viscous effects on Pitot tubes at low speeds. *J. R. Aero. Soc.* **58**, 837–839.
- MACMILLAN, F.A. 1957 Experiments on Pitot tubes in shear flow. *Ministry of Supply, Aero. Res. Council. R&M* 3028.
- MARUSIC, I., CHANDRAN, D., ROUHI, A., FU, M., WINE, D., HOLLOWAY, B., CHUNG, D. & SMITS, A.J. 2021 An energy-efficient pathway to turbulent drag reduction. *Nature Commun.* **12** (1), 5805.
- MARUSIC, I., CHAUHAN, K.A., KULANDAIVELU, V. & HUTCHINS, N. 2015 Evolution of zero-pressure-gradient boundary layers from different tripping conditions. *J. Fluid Mech.* **783**, 379–411.
- MARUSIC, I. & KUNKEL, G.J. 2003 Streamwise turbulence intensity formulation for flat-plate boundary layers. *Phys. Fluids* **15**, 2461–2464.
- MARUSIC, I., MATHIS, R. & HUTCHINS, N. 2010 Predictive model for wall-bounded turbulent flow. *Science* **329**, 193–196.
- MARUSIC, I., MONTY, J.P., HULTMARK, M. & SMITS, A.J. 2013 On the logarithmic region in wall turbulence. *J. Fluid Mech.* **716**, R3.
- MARUSIC, I., UDDIN, M. & PERRY, A.E. 1997 Similarity law for the streamwise turbulence intensity in zero-pressure-gradient turbulent boundary layers. *Phys. Fluids* **12**, 3718–3726.
- MATHIS, R., MARUSIC, I., CHERNYSHENKO, S.I. & HUTCHINS, N. 2013 Estimating wall-shear-stress fluctuations given an outer region input. *J. Fluid Mech.* **715**, 163–180.
- MCKEON, B.J., LI, J., JIANG, W., MORRISON, J.F. & SMITS, A.J. 2003 Pitot probe corrections in fully developed turbulent pipe flow. *Meas. Sci. Tech.* **14** (8), 1449–1458.
- MCKEON, B.J., LI, J., JIANG, W., MORRISON, J.F. & SMITS, A.J. 2004 Further observations on the mean velocity distribution in fully developed pipe flow. *J. Fluid Mech.* **501**, 135–147.
- MCKEON, B.J. & SMITS, A.J. 2002 Static pressure correction in high Reynolds number fully developed turbulent pipe flow. *Meas. Sci. Tech.* **13**, 1608–1614.
- MENEVEAU, C. & MARUSIC, I. 2013 Generalized logarithmic law for high-order moments in turbulent boundary layers. *J. Fluid Mech.* **719**, R1.
- METZGER, M.M., KLEWICKI, J.C., BRADSHAW, K.L. & SADR, R. 2001 Scaling the near-wall axial turbulent stress in the zero pressure gradient boundary layer. *Phys. Fluids* **13** (6), 1819–1821.
- MILLIKAN, C.B. 1938 A critical discussion of turbulent flows in channels and circular tubes. In *Proceedings of the 5th International Congress for Applied Mechanics*, vol. 386.
- MONKEWITZ, P. 2021 Asymptotics of stream-wise Reynolds stress in wall turbulence. *J. Fluid Mech.* **931**, A22.

- MORRISON, J.F., JIANG, W., MCKEON, B.J. & SMITS, A.J. 2002 Reynolds number dependence of streamwise velocity spectra in turbulent pipe flow. *Phys. Rev. Lett.* **88**, 214501.
- MORRISON, J.F., MCKEON, B.J., JIANG, W. & SMITS, A.J. 2004 Scaling of the streamwise velocity component in turbulent pipe flow. *J. Fluid Mech.* **508**, 99–131.
- MORRISON, J.F., VALLIKIVI, M. & SMITS, A.J. 2016 The inertial subrange in turbulent pipe flow: centreline. *J. Fluid Mech.* **788**, 602–613.
- MOSER, R.D., KIM, J. & MANSOUR, N.N. 1999 Direct numerical simulation of turbulent channel flow up to $Re_\tau = 590$. *Phys. Fluids* **11** (4), 943–945.
- NAGIB, H.M. & CHAUHAN, K.A. 2008 Variations of von Kármán coefficient in canonical flows. *Phys. Fluids* **20**, 101518.
- NAUGHTON, J.W. & SHEPLAK, M. 2002 Modern developments in shear-stress measurement. *Prog. Aerosp. Sci.* **38** (6-7), 515–570.
- NIKURADSE, J. 1932 Gesetzmäßigkeiten der turbulenten Strömung in glatten Röhren. Translated as Laws of turbulent flow in smooth pipes. *VDI Forschungsheft Arb. Ing.-Wes.*, vol. 356, also NACA TT F-10 356.
- OBERLACK, M., HOYAS, S., KRAHEBERGER, S. & ALCÁNTARA-ÁVILA, F. 2022 Turbulence statistics of arbitrary moments of wall-bounded shear flows: A symmetry approach. *Phys. Rev. Lett.* **128**, 024502.
- ÖRLÜ, R., FIORINI, T., SEGALINI, A., BELLANI, G., TALAMELLI, A. & ALFREDSSON, P.H. 2017 Reynolds stress scaling in pipe flow turbulence — first results from CICLOPE. *Philos. Trans. A Math. Phys. Engng Sci.* **375** (2089), 20160187.
- PERRY, A.E. 1982 *Hot-Wire Anemometry*. Oxford University Press.
- PERRY, A.E. & ABELL, C.J. 1977 Asymptotic similarity of turbulence structures in smooth- and rough-walled pipes. *J. Fluid Mech.* **79**, 785–799.
- PERRY, A.E., HENBEST, S.M. & CHONG, M.S. 1986 A theoretical and experimental study of wall turbulence. *J. Fluid Mech.* **165**, 163–199.
- PERRY, A.E. & LI, J.D. 1990 Experimental support for the attached-eddy hypothesis in zero-pressure-gradient turbulent boundary layers. *J. Fluid Mech.* **218**, 405–438.
- PIQUÉ, A., MILLER, M.A. & HULTMARK, M. 2020 Characterization of the wake behind a horizontal-axis wind turbine (HAWT) at very high Reynolds numbers. *J. Phys.: Conf. Ser.* **1618**, 062039. IOP Publishing.
- PIROZZOLI, S., ROMERO, J., FATICA, M., VERZICCO, R. & ORLANDI, P. 2021 One-point statistics for turbulent pipe flow up to $Re_\tau \approx 6000$. *J. Fluid Mech.* **926**, A28.
- POPE, S.B. 2000 *Turbulent Flows*. Cambridge University Press.
- PRANDTL, L. 1925 Bericht über untersuchungen zur ausgebildeten turbulenz. *Z. Angew. Math. Mech.* **5** (2), 136–139.
- ROSENBERG, B.J., HULTMARK, M., VALLIKIVI, M., BAILEY, S.C.C. & SMITS, A.J. 2013 Turbulence spectra in smooth- and rough-wall pipe flow at extreme Reynolds numbers. *J. Fluid Mech.* **731**, 46–63.
- SADEGHI, H., LAVOIE, P. & POLLARD, A. 2018 Effects of finite hot-wire spatial resolution on turbulence statistics and velocity spectra in a round turbulent free jet. *Exp. Fluids* **59** (3), 40.
- SAMIE, M., MARUSIC, I., HUTCHINS, N., FU, M.K., FAN, Y., HULTMARK, M. & SMITS, A.J. 2018 Fully resolved measurements of turbulent boundary layer flows up to $Re_\tau = 20\,000$. *J. Fluid Mech.* **851**, 391–415.
- SCHLICHTING, H. 1979 *Boundary-Layer Theory*, 7th edn. McGraw-Hill.
- SCHULTZ, M.P. & FLACK, K.A. 2013 Reynolds-number scaling of turbulent channel flow. *Phys. Fluids* **25** (2), 025104.
- SEGALINI, A., RÜEDI, J.-D. & MONKEWITZ, P.A. 2015 Systematic errors of skin-friction measurements by oil-film interferometry. *J. Fluid Mech.* **773**, 298–326.
- SHE, Z.-S. & LEVEQUE, E. 1994 Universal scaling laws in fully developed turbulence. *Phys. Rev. Lett.* **72** (3), 336.
- SILLERO, J.A., JIMÉNEZ, J. & MOSER, R.D. 2013 One-point statistics for turbulent wall-bounded flows at Reynolds numbers up to $\delta^+ \approx 2000$. *Phys. Fluids* **25** (10), 105102.
- SINHUBER, M., BEWLEY, G.P. & BODENSCHATZ, E. 2017 Dissipative effects on inertial-range statistics at high Reynolds numbers. *Phys. Rev. Lett.* **119** (13), 134502.
- SMITS, A.J. 2020 Some observations on Reynolds number scaling in wall-bounded flows. *Phys. Rev. Fluids* **5** (11), 110514.
- SMITS, A.J. & HULTMARK, M. 2014 Nanoscale instrumentation for measuring turbulence. In *Proceedings of the 19th Australasian Fluid Mechanics Conference*, vol. 19, pp. 11–17. University of Melbourne.
- SMITS, A.J., HULTMARK, M., LEE, M., PIROZZOLI, S. & WU, X. 2021 Reynolds stress scaling in the near-wall region of wall-bounded flows. *J. Fluid Mech.* **926**, A31.
- SMITS, A.J., MONTY, J., HULTMARK, M., BAILEY, S.C.C., HUTCHINS, M. & MARUSIC, I. 2011 Spatial resolution correction for turbulence measurements. *J. Fluid Mech.* **676**, 41–53.

- SMITS, A.J., PERRY, A.E. & HOFFMANN, P.H. 1978 The response to temperature fluctuations of a constant current hot-wire anemometer. *J. Phys. E: Sci. Instrum.* **11**, 909–914.
- SMOLIAKOV, A.V. & TKACHENKO, V.M. 1983 *The Measurement of Turbulent Fluctuations: An Introduction to Hot-Wire Anemometry and Related Transducers*, p. 311. Springer-Verlag.
- SREENIVASAN, K.R. & SAHAY, A. 1997 The persistence of viscous effects in the overlap region and the mean velocity in turbulent pipe and channel flows. In *Self-Sustaining Mechanisms of Wall Turbulence* (ed. R. Panton), pp. 253–272. Computational Mechanics Publications.
- TOWNSEND, A.A. 1976 *The Structure of Turbulent Shear Flow*. Cambridge University Press.
- TROPEA, C. 1995 Laser Doppler anemometry: recent developments and future challenges. *Meas. Sci. Tech.* **6** (6), 605.
- VALLIKIVI, M., GANAPATHISUBRAMANI, B. & SMITS, A.J. 2015a Spectral scaling in boundary layers and pipes at very high Reynolds numbers. *J. Fluid Mech.* **771**, 303–326.
- VALLIKIVI, M., HULTMARK, M., BAILEY, S.C.C. & SMITS, A.J. 2011 Turbulence measurements in pipe flow using a nano-scale thermal anemometry probe. *Exp. Fluids* **51**, 1521–1527.
- VALLIKIVI, M., HULTMARK, M. & SMITS, A.J. 2015b Turbulent boundary layer statistics at very high Reynolds number. *J. Fluid Mech.* **779**, 371–389.
- VALLIKIVI, M. & SMITS, A.J. 2014 Fabrication and characterization of a novel nano-scale thermal anemometry probe. *J. Microelectromech. Syst.* **23** (4), 899–907.
- VINCENTI, P., KLEWICKI, J., MORRILL-WINTER, C., WHITE, C.M. & WOSNIK, M. 2013 Streamwise velocity statistics in turbulent boundary layers that spatially develop to high Reynolds number. *Exp. Fluids* **54** (12), 1629.
- VINUESA, R., NOORANI, A., LOZANO-DURÁN, A., EL KHOURY, G.K., SCHLATTER, P., FISCHER, P.F. & NAGIB, H.M. 2014 Aspect ratio effects in turbulent duct flows studied through direct numerical simulation. *J. Turbul.* **15** (10), 677–706.
- WEI, T., FIFE, P., KLEWICKI, J.C. & MCMURTRY, P. 2005 Properties of the mean momentum balance in turbulent boundary layer, pipe and channel flows. *J. Fluid Mech.* **522**, 303–327.
- WESTERWEEL, J., ELSINGA, G.E. & ADRIAN, R.J. 2013 Particle image velocimetry for complex and turbulent flows. *Annu. Rev. Fluid Mech.* **45**, 409–436.
- WILLERT, C.E., SORIA, J., STANISLAS, M., KLINNER, J., AMILI, O., EISFELDER, M., CUVIER, C., BELLANI, G., FIORINI, T. & TALAMELLI, A. 2017 Near-wall statistics of a turbulent pipe flow at shear Reynolds numbers up to 40 000. *J. Fluid Mech.* **826**, R5.
- WILLIAMS, O. 2014 Density effects on turbulent boundary layer structure: from the atmosphere to hypersonic flow. PhD thesis, Princeton University, Princeton, NJ.
- WILLIAMS, O., VAN BUREN, T. & SMITS, A.J. 2015 A new method for measuring turbulent heat fluxes using PIV and fast-response cold-wires. *Exp. Fluids* **56** (7), 142.
- WILLIAMS, O.J.H., SAHOO, D., BAUMGARTNER, M.L. & SMITS, A.J. 2018 Experiments on the structure and scaling of hypersonic turbulent boundary layers. *J. Fluid Mech.* **834**, 237–270.
- WOSNIK, M., CASTILLO, L. & GEORGE, W.K. 2000 A theory for turbulent pipe and channel flows. *J. Fluid Mech.* **421**, 115–145.
- WYNGAARD, J.C. 1968 Measurement of small-scale turbulence structure with hot-wires. *J. Phys. E: Sci. Instrum.* **2**, 1105–1108.
- YAKHOT, V., BAILEY, S.C.C. & SMITS, A.J. 2010 Scaling of global properties of turbulence and skin friction in pipe and channel flows. *J. Fluid Mech.* **652**, 65–73.
- YAMAMOTO, Y. & TSUJI, Y. 2018 Numerical evidence of logarithmic regions in channel flow at $Re_\tau = 8000$. *Phys. Rev. Fluids* **3** (1), 012602.
- YAO, J., SCHLATTER, P., REZAEIRAVESH, S. & HUSSAIN, F. 2021 Direct numerical simulation of turbulent pipe flow up to $Re_\tau = 5200$. In *Bulletin of American Physical Society*, 66.
- ZAGAROLA, M.V. & SMITS, A.J. 1998a Mean-flow scaling of turbulent pipe flow. *J. Fluid Mech.* **373**, 33–79.
- ZAGAROLA, M.V. & SMITS, A.J. 1998b A new mean velocity scaling for turbulent boundary layers. *ASME Paper FEDSM98-4950*.
- ZANOUN, E.-S., DURST, F. & NAGIB, H. 2003 Evaluating the law of the wall in two-dimensional fully developed turbulent channel flows. *Phys. Fluids* **15** (10), 3079–3089.
- ZIMMERMAN, S., *et al.* 2019 A comparative study of the velocity and vorticity structure in pipes and boundary layers at friction Reynolds numbers up to 10^4 . *J. Mech.* **869**, 182–213.